JBC RESEARCH ARTICLE

Structure, dynamics, and regulation of TRF1-TIN2-mediated trans- and cis-interactions on telomeric DNA

Received for publication, March 7, 2021, and in revised form, July 30, 2021 Published, Papers in Press, August 14, 2021,
https://doi.org/10.1016/j.jbc.2021.101080

Hai Pan[1], Parminder Kaur[1,2], Ryan Barnes[3], Ariana C. Detwiler[3], Samantha Lynn Sanford[3], Ming Liu[1], Pengning Xu[1], Chelsea Mahn[1], Qingyu Tang[4], Pengyu Hao[1], Dhruv Bhattaram[5], Changjiang You[6], Xinyun Gu[7], Warren Lu[8], Jacob Piehler[6], Guozhou Xu[4], Keith Weninger[1], Robert Riehn[1], Patricia L. Opresko[3,9], and Hong Wang[1,2,10,*]

From the [1]Physics Department and [2]Center for Human Health and the Environment, North Carolina State University, Raleigh, North Carolina, USA; [3]Department of Environmental and Occupational Health, UPMC Hillman Cancer Center, University of Pittsburgh, Pittsburgh, Pennsylvania, USA; [4]Department of Molecular and Structural Biochemistry, North Carolina State University, Raleigh, North Carolina, USA; [5]Department of Biomedical Engineering, Georgia Institute of Technology & Emory University of Medicine, Atlanta, Georgia, USA; [6]Department of Biology/Chemistry, Universität Osnabrück, Osnabrück, Germany; [7]College of Art and Sciences and [8]Department of Pathology at NYU Grossman School of Medicine, New York University, New York City, New York, USA; [9]Molecular Biophysics and Structural Biology Graduate Program, Carnegie Mellon University and the University of Pittsburgh, Pittsburgh, Pennsylvania, USA; and [10]Toxicology Program, North Carolina State University, Raleigh, North Carolina, USA

Edited by Patrick Sung

TIN2 is a core component of the shelterin complex linking double-stranded telomeric DNA-binding proteins (TRF1 and TRF2) and single-strand overhang-binding proteins (TPP1-POT1). *In vivo*, the large majority of TRF1 and TRF2 exist in complexes containing TIN2 but lacking TPP1/POT1; however, the role of TRF1-TIN2 interactions in mediating interactions with telomeric DNA is unclear. Here, we investigated DNA molecular structures promoted by TRF1-TIN2 interaction using atomic force microscopy (AFM), total internal reflection fluorescence microscopy (TIRFM), and the DNA tightrope assay. We demonstrate that the short (TIN2S) and long (TIN2L) isoforms of TIN2 facilitate TRF1-mediated DNA compaction (*cis*-interactions) and DNA-DNA bridging (*trans*-interactions) in a telomeric sequence- and length-dependent manner. On the short telomeric DNA substrate (six TTAGGG repeats), the majority of TRF1-mediated telomeric DNA-DNA bridging events are transient with a lifetime of ~1.95 s. On longer DNA substrates (270 TTAGGG repeats), TIN2 forms multiprotein complexes with TRF1 and stabilizes TRF1-mediated DNA-DNA bridging events that last on the order of minutes. Preincubation of TRF1 with its regulator protein Tankyrase 1 and the cofactor NAD^+ significantly reduced TRF1-TIN2 mediated DNA-DNA bridging, whereas TIN2 protected the disassembly of TRF1-TIN2 mediated DNA-DNA bridging upon Tankyrase 1 addition. Furthermore, we showed that TPP1 inhibits TRF1-TIN2L-mediated DNA-DNA bridging. Our study, together with previous findings, supports a molecular model in which protein assemblies at telomeres are heterogeneous with distinct subcomplexes and full shelterin complexes playing distinct roles in telomere protection and elongation.

Telomeres are nucleoprotein structures that prevent the degradation or fusion of the ends of linear chromosomes, which are threatened by at least seven distinct DNA damage response (DDR) pathways (1–3). Human telomeres contain ~2–20 kb of TTAGGG repeats and a G-rich 3′ overhang of ~50–400 nt in length (1, 4). In humans, a specialized six-protein shelterin complex consisting of TRF1, TRF2, RAP1, TIN2, TPP1, and POT1 binds specifically to the unique sequence and structure at telomeres to protect chromosome ends. Prevention of telomeres from being falsely recognized as double-strand DNA breaks and regulation of DNA repair protein access depend on the biochemical activities of shelterin proteins and their collaborative actions with other proteins involved in the genome maintenance pathways (5–9). Extensive telomere shortening or dramatic telomere loss due to DNA damage causes telomere deprotection, which triggers cell senescence and aging-related pathologies (10, 11).

The main protein–protein and protein–DNA interactions at telomeres have been investigated using crystallography, biochemical assays, yeast two-hybrid systems, coimmunoprecipitation, as well as visualization of shelterin subcomponents *in vitro* and *in vivo* using fluorescence imaging (3). Among shelterin components, both TRF1 and TRF2 specifically recognize double-stranded telomeric DNA through the Myb/SANT domain facilitated by homodimerization through the TRFH domain (12, 13). However, TRF1 and TRF2 display distinct DNA-binding properties and functions. TRF1 and TRF2 contain an acidic and a basic domain, respectively, at their N-termini (14). TRF2 prevents Mre11/Rad50/Nbs1-dependent ATM kinase signaling, classical nonhomologous end-joining (NHEJ), as well as alternative nonhomologous end-joining (alt-NHEJ) pathways at telomeres. These distinct functions of TRF2 are believed to be mediated through its activities in promoting and stabilizing T-loops, in which the 3′

* For correspondence: Hong Wang, hong_wang@ncsu.edu.

single-stranded overhang invades the upstream double-stranded telomeric region (15–18). In comparison, TRF1 represses telomere fragility by preventing DNA replication fork stalling at telomeres (19) and promotes parallel pairing of telomeric DNA tracts (20, 21). A flexible domain in TRF1 enables the two Myb domains in the TRF1 dimer to interact with DNA independently and to mediate looping of telomeric DNA (22).

TIN2 itself does not have binding affinity to either double-stranded or single-stranded DNA (23). However, it is a core shelterin component that bridges double-stranded (TRF1 and TRF2) and single-stranded telomeric DNA-binding proteins (TPP1-POT1) (24–28). Crystal structures revealed the interfaces between TRF1-TIN2, TRF2-TIN2, and TPP1-TIN2 (29, 30). TIN2 stabilizes both TRF1 and TRF2 at telomeres (31, 32). The loss of the TRF1 or TRF2-binding domains in TIN2 triggers a DNA damage response (33). Binding of TPP1 to TIN2 is required for POT1-mediated telomere protection (34). As an integral component of the "TIN2/TPP1/POT1 processivity complex," TIN2 functions together with TPP1/POT1 to stimulate telomerase processivity (35). Furthermore, TIN2 directly interacts with the cohesin subunit SA1 and plays a key role in a distinct SA1-TRF1-TIN2-mediated sister telomere cohesion pathway that is largely independent of the cohesin ring subunits (8, 36). Binding of TRF1-TIN2 to telomeres is regulated by the poly(ADP-ribose) polymerase Tankyrase 1 (37). ADP-ribosylation of TRF1 by Tankyrase 1 reduces its binding to telomeric DNA *in vitro*, and the depletion of Tankyrase 1 using siRNA leads to mitotic arrest and persistent telomere cohesion that can be rescued by depletion of TIN2 (8, 36, 38).

Three distinct TIN2 isoforms have been identified in human cell lines (35, 39, 40) that include TIN2S (354 AAs), TIN2L (451 AAs), and TIN2M (TIN2 medium, 420 AAs). TIN2S, TIN2L, and TIN2M share the same TRF1, TRF2, and TPP1-binding domains and localize to telomeres (23, 35, 39). Consistent with its key role in telomere maintenance, germline inactivation of TIN2 in mice is embryonic lethal (41). Removal of TIN2 leads to the formation of telomere dysfunction-induced foci (TIFs). Importantly, clinical studies further highlight the biological significance of TIN2 in telomere protection (42, 43). *TINF2*, which encodes TIN2, is the second most frequently mutated gene in the telomere elongation and protection disorder dyskeratosis congenita (DKC). DKC-associated TIN2 mutations are most frequently *de novo* and cluster at a highly conserved region near the end of its TRF1-binding domain.

Two decades of research since the first discovery of TIN2 have shed light on protein-interaction networks around TIN2 and its multifaceted roles in telomere maintenance. However, since TIN2 itself does not directly bind to DNA and instead serves as a "mediator/enhancer" for shelterin and telomerase activities, defining TIN2's distinct function at the molecular level has been challenging. The bottleneck for studying TIN2 lies in the fact that results from bulk biochemical assays do not fully reveal the heterogeneity and dynamics of the protein–protein and protein–DNA interactions. Furthermore, cell-based assays only provide information on the outcomes from downstream effectors after the knocking down of TIN2 that also removes TRF1 and TRF2 from telomeres. These approaches do not allow us to investigate the molecular structures and dynamics in which TIN2 directly participates. *In vivo*, the amount of TIN2 is sufficient for binding every TRF1 and TRF2 molecule (44), while TPP1 and POT1 are ~10-fold less than TRF1 and TIN2. Thus, it is important to study the DNA-binding properties of TRF1-TIN2 complexes. To fill this important knowledge gap, we applied complementary single-molecule imaging platforms, including atomic force microscopy (AFM) (45–47), total internal reflection fluorescence microscopy (TIRFM) (48), and the DNA tight-rope assay to monitor TRF1-TIN2-mediated DNA compaction and DNA-DNA bridging (49–51). Through using DNA substrates on different length scales (6 and 270 TAAGGG repeats), these imaging platforms provide complementary results demonstrating that both TIN2S and TIN2L facilitate TRF1-mediated DNA compaction (*cis*-interactions) and DNA-DNA bridging (*trans*-interactions) in a telomeric sequence- and length-dependent manner. In some cases, TRF1-TIN2 is capable of mediating the bridging of multiple copies of telomeric DNA fragments. Importantly, our results demonstrate that TIN2 protects the disassembly of TRF1-TIN2-mediated DNA-DNA bridging by Tankyrase 1. In addition, the N-terminal domain of TPP1 inhibits TRF1-TIN2-mediated DNA-DNA bridging.

In summary, this study uncovered the unique biophysical function of TIN2 as a telomeric architectural protein, acting together with TRF1 to mediate interactions between distant telomeric sequences. Tankyrase 1 and TPP1 regulate TRF1-TIN2-mediated DNA-DNA bridging. Furthermore, this work establishes a unique combination of single-molecule imaging platforms for future examination of TIN2 disease variants and provides a new direction for investigating molecular mechanisms underlying diverse TIN2 functions.

Results

TRF1-TIN2 promotes telomeric DNA compaction and DNA-DNA bridging

A previous study suggested that TIN2 modulates the bridging of telomeric DNA by TRF1 (31). However, the bulk biochemical assays using short telomeric DNA (six telomeric repeats) did not provide information regarding the structure and dynamics of the TRF1-TIN2-DNA complex. To investigate the molecular function of TIN2, we applied AFM imaging to investigate how TIN2 affects the telomeric DNA-DNA pairing mediated by TRF1 at the single-molecule level on longer telomeric DNA substrates (270 TTAGGG repeats). We purified TRF1 (Fig. S1*A*) and obtained TIN2S (1–354 amino acids, 39.4 kDa) and TIN2L (1–451 amino acids, 50.0 kDa) proteins purified from insect cells (Fig. 1*A* and Fig. S1*D*). Previously, we established an AFM imaging-based calibration method to investigate the oligomeric states and protein–protein interactions by correlating AFM volumes of proteins and their molecular weights (45, 47, 52). AFM volumes of

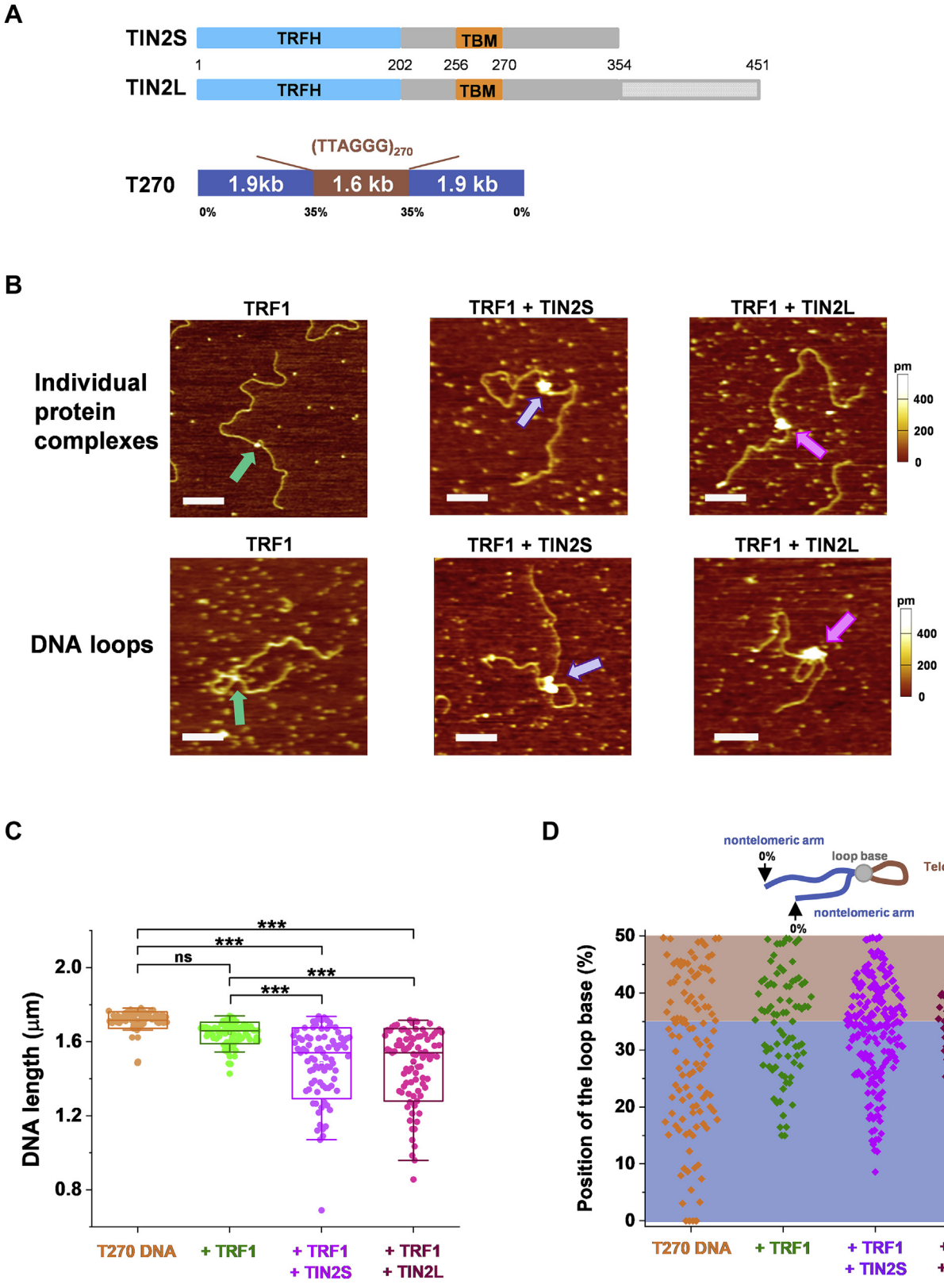

Figure 1. TRF1-TIN2 compact DNA and induce DNA looping in a telomeric DNA sequence-dependent manner. *A*, schematics of domain structures of TIN2S and TIN2L (*top panels*) and the linear T270 DNA substrate (*bottom panel*). *B*, representative AFM images of TRF1 (*left panels*), TRF1-TIN2S (*middle panels*), and TRF1-TIN2L (*right panels*) complexes on the linear T270 DNA, showing individual protein complexes (*arrows*, *top panels*) and protein-mediated DNA loops (*arrows*, *bottom panels*). XY scale bars: 200 nm. *C*, TRF1-TIN2 compacted the telomeric DNA. DNA length measurements for the linear T270 DNA alone (1.71 ± 0.05 μm, N = 90), T270 in the presence of TRF1 (1.64 ± 0.06 μm, N = 91), TRF1 and TIN2S (1.58 ± 0.11 μm, N = 85), or TRF1 and TIN2L (1.59 ± 0.1 μm, N = 89). Boxes represent ±SD. Error bars indicate ranges within 1.5QR. *D*, analysis of the TRF1, TRF1-TIN2S, and TRF1-TIN2L-mediated DNA loop positions on individual T270 DNA molecules. The loop position was measured from each DNA end (0%) to the loop base with two data points collected from one T270 DNA molecule. T270 only: N = 112; T270+TRF1: N = 84; T270+TRF1+TIN2S: N = 196; T270+TRF1+TIN2L: N = 224. $^{**}p < 0.01$ and $^{***}p < 0.001$.

TRF1 alone in solution showed two distinct peaks, which were consistent with TRF1 monomers (51 KDa) and dimers (102 KDa, Fig. S1*B*). In addition, based on the population of TRF1 under the monomer and dimer peaks (53), the estimated TRF1 dimer equilibrium dissociation constant (K_d) is 18.4 nM (Fig. S1*C*). Meanwhile, AFM volumes of purified TIN2S at 41.3 nm^3 (±28.3 nm^3) and TIN2L at 41.9 nm^3 (±12.8 nm^3) were consistent with the notion that TIN2 does not interact with itself (23), and TIN2 exists in a monomeric state in solution (Fig. S1*D*). Furthermore, we conducted size-exclusive chromatography using TRF1 and TIN2S and confirmed the presence of TRF1 dimers, TIN2 monomers, as well as the interaction between TRF1 and TIN2S in solution (Fig. S2). To further validate the activities of TIN2, we used electrophoresis mobility shift assays (EMSAs) to verify the interaction of TIN2 with TRF1 on a double-stranded telomeric DNA substrate (48 bp containing three TTAGGG repeats, Fig. S3, *A*–*C*). Consistent with previous studies (23), EMSA experiments showed that TIN2S and TIN2L did not directly bind to telomeric dsDNA (Fig. S3*A*). Both TRF1-TIN2S and TRF1-TIN2L induced a clear supershift of the telomeric DNA substrate compared with TRF1 alone (Complex III in Fig. S3, *B* and *C*), indicating the formation of stable TRF1-TIN2-telomeric DNA complexes.

Next, to study TRF1-TIN2 DNA binding at the single-molecule level, we used the linear DNA substrate (5.4 kb) that contains 1.6 kb (270 TTAGGG) telomeric repeats in the middle region that is 35%–50% from DNA ends (T270 DNA, Experimental procedures, Fig. 1*A*) (21, 49). Previously, AFM and electron microscopy imaging–based studies established that TRF1 specifically binds to the telomeric region and mediates DNA-DNA pairing (21, 22, 49). To study the function of TIN2, we preincubated TRF1 without or with TIN2 (either TIN2S or TIN2L), followed by the addition of linear T270 DNA and additional incubation for 10 min. The ratio of TRF1:telomere DNA measured in HeLa1.3 cells is approximately 1 TRF1:14.2 (TTAGGG) repeats (44). To investigate the effect of TIN2 on DNA binding by TRF1, we used TRF1:TIN2:DNA at 1:1:0.17 (300 nM: 300 nM: 50 nM). Based on the AFM height of TRF1 (0.48 ± 0.13 nm), we used an AFM height cutoff at 1 nm to select the protein complexes on T270 DNA that contained TIN2. Based on this selection criteria, we categorized the TRF1-TIN2-DNA complexes (N = 2837, combining TIN2S and TIN2L data), into three types: DNA molecules with individual protein complexes bound along the linear DNA contour (21.4% ± 6.2% of total DNA molecules); DNA molecules with a loop that is mediated by a protein complex (7.4% ± 4.6% of total DNA molecules, Fig. 1*B* and Table S1); and clusters of multiple T270 DNA fragments bridged by protein complexes (*trans*-interactions, 38.5 ± 3.7% of total DNA molecules, Fig. 2 and Table S1).

The majority of the individually bound TRF1-TIN2 protein complexes (55% for TIN2S and 75% for TIN2L) were located at the telomeric region (35%-50% from the closest DNA end) on the linear T270 DNA (Fig. S4*A*). The linear T270 DNA contour length in the presence of TRF1-TIN2 displayed broader distributions and was significantly ($p < 0.001$) shortened compared with DNA alone or DNA in the presence of only TRF1 (Fig. 1*C*). The AFM volumes of TRF1-TIN2 protein complexes on individual T270 DNA fragments were an order of magnitude larger than what was observed for TRF1 alone (Fig. S4, *B* and *C*). Although it is technically challenging to quantify numbers of protein molecules in individual protein–DNA complexes, these results demonstrated that TRF1-TIN2-DNA complexes contained multiple copies of TRF1 and TIN2. In addition, the distribution of TRF1-TIN2L complexes on the control linear nontelomeric DNA (noTel, 4.1 kb) was random and the lengths of noTel DNA were comparable in the absence or presence of TRF1-TIN2L (Fig. S5, *A*–*C*). In summary, these results established that TRF1-TIN2 specifically bind to the telomeric DNA sequences and compact telomeric DNA.

To verify that TRF1-TIN2 complexes mediate DNA looping (*cis*-interactions) specifically at the telomeric region, we quantified the position of the base of protein-mediated DNA loops by directly measuring the length of each DNA arm from the free DNA end to the base of the loop (Fig. 1*D*). We treated 35% (±3.5%) of the total contour length of T270 from the nearest end as telomeric and nontelomeric region boundaries (Fig. S6). TRF1-TIN2-mediated DNA looping was positioned either within the telomeric region (33.7% for TIN2S and 25.1% for TIN2L), between telomeric and nontelomeric regions (63.2% for TIN2S and 66.1% for TIN2L), or between two nontelomeric arms (3.1% for TIN2S and 8.8% for TIN2L). These results demonstrated that TRF1 and TIN2 together mediated DNA looping in a telomeric sequence-dependent manner.

Furthermore, TRF1-TIN2S and TRF1-TIN2L formed large complexes that bridged multiple strands of linear T270 DNA molecules in a time and telomeric sequence-dependent manner (Fig. 2, *A*–*C*). After 15 min of incubation, a significant percentage of linear T270 DNA molecules (34.8% ± 3.5% for TRF1-TIN2S and 42.5% ± 5.1% for TRF1-TIN2L) resided in protein–DNA clusters with more than two T270 fragments (Fig. 2*D*). In addition, the N-terminal deletion mutant of TIN2S lacking amino acids 1–196 (TIN2S-13) did not form the higher-order Complex III in the presence of TRF1 (Fig. S3*D*). Consistent with these results, the percentage of T270 DNA in protein–DNA clusters induced by TRF1-TIN2S-13 was significantly less compared with TRF1-TIN2 (17.4% ± 3.1% after 20 min of incubation, N = 1139, Fig. S3*E*). The sizes of protein complexes when both TRF1 and TIN2 were present (TRF1-TIN2S: 6816 ± 4788 nm^3, TRF1-TIN2L: 7286 ± 5229 nm^3, Fig. S7) were at least 45 times greater than volumes of a TRF1 dimer (~105 nm^3) and TIN2 monomer (~41 nm^3) combined together (Fig. S1). In comparison, for TRF1 alone with T270 DNA or noTel DNA in the presence of TRF1 and TIN2L, complexes with clusters of multiple DNA fragments bridged by proteins were significantly fewer (Fig. 2, *C* and *D* and Table S1). Collectively, results from AFM imaging established that both TIN2S and TIN2L facilitate *cis*-interactions leading to DNA compaction and *trans*-interactions leading to DNA-DNA bridging in a telomeric sequence-dependent

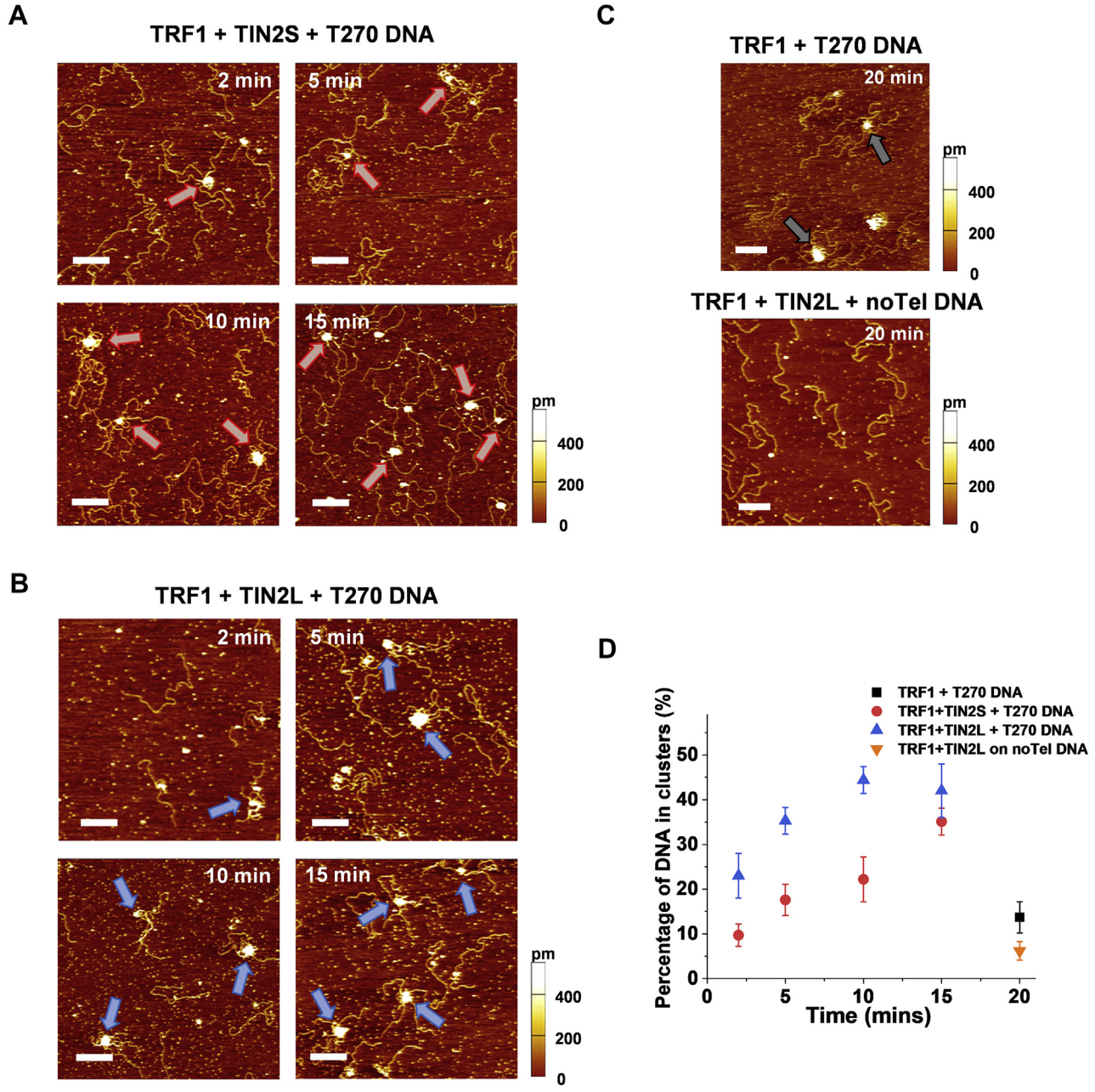

Figure 2. TRF1-TIN2 form large complexes and bridge multiple dsDNA fragments in a telomeric sequence and time-dependent manner. *A* and *B*, representative AFM images of TRF1-TIN2S (*A*) and TRF1-TIN2L (*B*) complexes showing bridging of multiple fragments of T270 DNA (5.4 kb) after incubation for 2 min, 5 min, 10 min, and 15 min. *Arrows* point to complexes containing more than two T270 fragments. *C*, representative AFM images from control experiments using TRF1 alone with the linear T270 DNA, and TRF1-TIN2L with the nontelomeric DNA (noTel, 4.1 kb) after incubation for 15 min. XY scale bars: 500 nm. *D*, percentages of DNA molecules in the clusters containing more than two DNA fragments bridged by TRF1 on T270 DNA, and TRF1-TIN2L on nontelomeric DNA after 20 min of incubation, TRF1-TIN2S or TRF1-TIN2L on T270 DNA at different incubation times. Each data set: total DNA molecules: N = 591 to 1560. Error bars: SEM from three independent experiments.

manner. The N-terminal domain of TIN2 plays a key role in facilitating TRF1-mediated DNA-DNA bridging.

TIN2 increases TRF1-mediated telomeric DNA-DNA bridging lifetimes

To gain mechanistic insight into how TIN2 influences DNA-DNA bridging by TRF1, we applied single-molecule TIRFM fluorescence imaging to monitor DNA-DNA bridging in real time. First, Cy5-labeled and biotinylated double-stranded telomeric DNA substrates containing six TTAGGG repeats were anchored onto PEGylated quartz slides through biotin–streptavidin interactions (Experimental procedures, Fig. 3*A*). Then, we introduced TRF1 or TRF1-TIN2 (TIN2S or TIN2L, 100 nM each protein) into the flow cell, followed by washing with the imaging buffer. After 10 min of incubation, we added the telomeric Cy3-DNA with six TTAGGG repeats but lacking biotin as free DNA from solution (5 nM) along with proteins (TRF1 either with or without TIN2) into the flow cell. To reveal the dynamics of the protein-

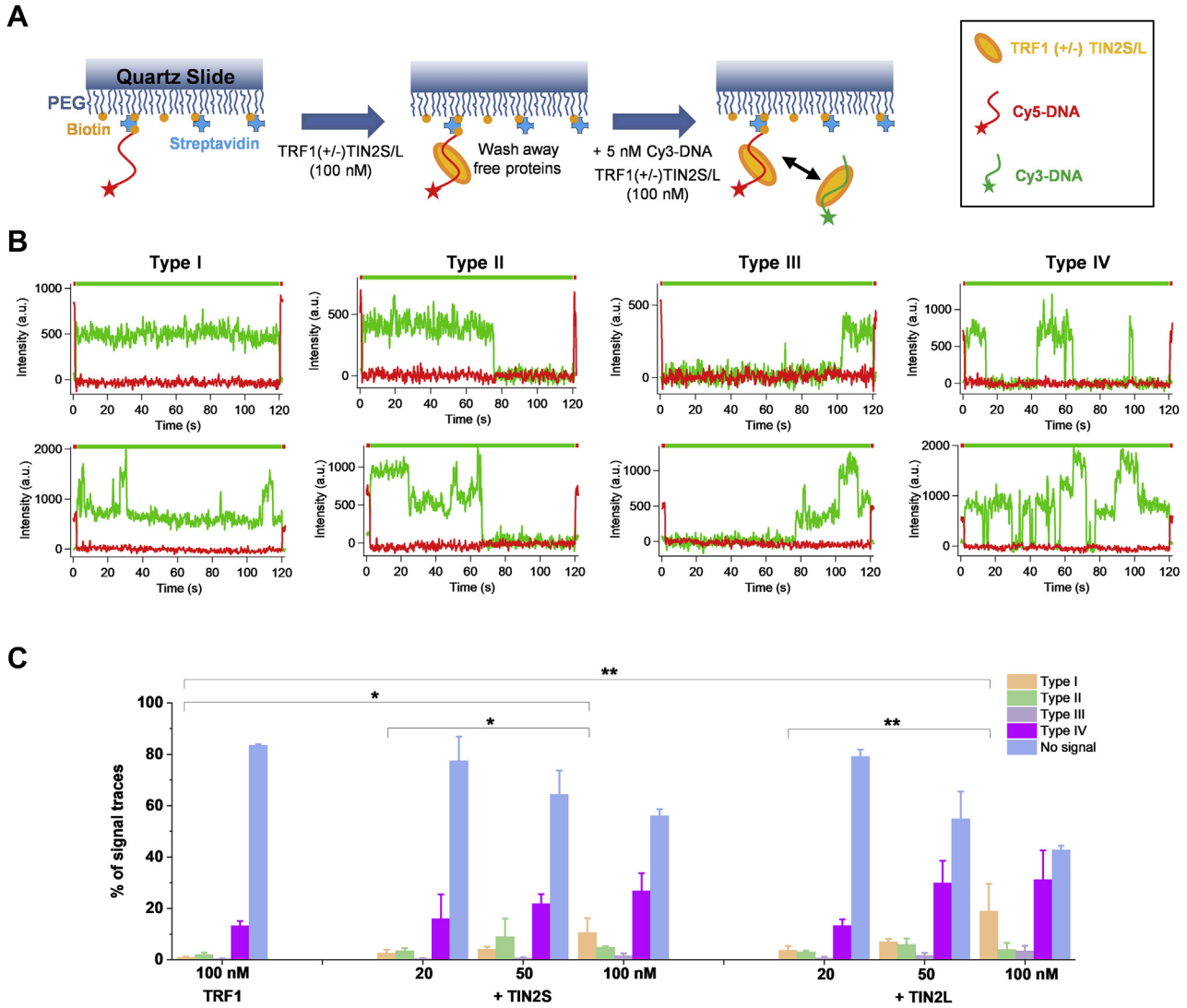

Figure 3. TIN2 facilitates TRF1-mediated bridging of telomeric dsDNA revealed by TIRFM imaging. *A*, schematics of the experimental setup for monitoring DNA-DNA bridging (*trans*-interactions) mediated by TRF1-TIN2 using TIRFM imaging. *B*, four types of single-molecule traces of TRF1-TIN2 mediated DNA-DNA bridging events observed using TIRFM imaging. One (*top panels*) or multiple (*bottom panels*) Cy3-DNA molecules were bridged to the surface-anchored Cy5-DNA. The lines on the top indicate laser excitation sequence. *C*, the percentages of each type of telomeric DNA-DNA bridging events with TRF1 alone, or TRF1 with increasing concentrations of TIN2S or TIN2L observed using TIRFM. Each data set was based on more than 1000 fluorescence traces collected from three to four independent experiments. *$p < 0.05$ and **$p < 0.01$.

mediated colocalization of the Cy5-and Cy3-DNA (*trans*-interactions), we illuminated the slide surface with a red laser, followed by a green laser, to excite the Cy5 and Cy3 fluorophores, respectively, and captured 120-s movies. To monitor whether the free Cy3-DNA from the solution was bridged by proteins to the Cy5-DNA anchored onto the surface, the spots that displayed signals in the Cy5 channel were located first. Then, a map was used to locate the spots in the Cy3-DNA channel (Fig. S8*A*) and to reveal the temporal dynamics of the colocalization of Cy5-and Cy3-DNA (Fig. 3).

We conducted a series of control experiments under the same experimental conditions to validate that Cy3-and Cy5-DNA colocalization was mediated by proteins in a telomeric sequence-dependent manner and not through nonspecific interactions (Fig. S8, *B–E*). Under the conditions either without proteins (Fig. S8*B*), without Cy5-telomeric DNA on the surface (Fig. S8*C*), or with Cy3-DNA containing scrambled sequences (Fig. S8, *D* and *E*), Cy3-Cy5 DNA colocalization or Cy3 signals at randomly selected spots were ~1.5%–5% of total traces/spots.

To investigate whether or not TIN2 influences the efficiency and dynamics of TRF1-mediated telomeric DNA-DNA bridging, we directly compared Cy5-Cy3 colocalization signals when only TRF1 or both TRF1 and TIN2 were present. When the telomeric Cy5-DNA was immobilized on the surface and TRF1 alone (100 nM) was present in the flow cell, the percentage of Cy5 traces colocalized with telomeric Cy3-DNA signals was 16.6% (±0.5%, N = 2369). This percentage increased to over 50.6% (±7.3%, N = 3540) in the presence of both TRF1 and TIN2 (TIN2S or TIN2L). To further interpret the data, we classified the traces with Cy5-Cy3 DNA colocalization signals into four types (Fig. 3*B*). Type I: stable bridging

in which the Cy3-DNA in solution was bridged to the Cy5-DNA on the surface from the beginning to the end of the movie; Type II: the Cy3-DNA was bridged to the Cy5-DNA at the beginning of the movies and then released (or photobleached); Type III: Cy3-DNA was bridged to Cy5 DNA during the middle of the movies and did not dissociate from each other till the end of the movies; Type IV: multiple transient DNA-DNA bridging and releasing events. It is worth noting that we categorized the traces based on Cy3-DNA signal duration. Based on the Cy3 signal intensities, each category includes events with either one or multiple Cy3-DNA molecules bridged to the surface-anchored Cy5-DNA (Fig. 3*B*). When TRF1 (100 nM) alone was present in the chamber, only 1.0% (±0.3%) of all event traces showed Type I stable bridging. The dwell time and dissociation time of Cy5-Cy3 DNA bridging Type IV events were 1.95 s and 3.38 s, respectively, for TRF1 (Fig. S9). In the presence of TRF1-TIN2 (TIN2S or TIN2L), there was an additional population with longer dwell times (>40 s, Fig. S9*B*). Notably, over 80% of fluorescent signals from DNA molecules persisted after 40-s of laser illumination, excluding the possibility that the Type IV events were from photobleaching (Fig. S8*F*).

Next, to investigate if the stabilization of TRF1-mediated DNA-DNA bridging is TIN2 concentration-dependent, we quantified the percentages of different types of events at a fixed TRF1 concentration (100 nM), but varying TIN2 concentrations (25 nM, 50 nM, and 100 nM) (Fig. 3*C*). Results from these experiments showed a clear correlation between increasing TIN2 concentrations and higher percentages of DNA-DNA bridging events. The total percentage of telomeric DNA-DNA bridging signals increased significantly ($p < 0.05$) from 22.6% (±1.6%) at 25 nM to 43.9% (±2.6%) for TIN2S (100 nM) and from 20.9% (±0.4%) at 25 nM to 57.5% (±5.7%) at 100 nM for TIN2L. Furthermore, the percentages of Type I stable bridging traces were significantly increased with higher concentrations of TIN2S (from 2.6% ± 1.3% at 25 nM TIN2S to 10.6% ± 5.6% at 100 nM TIN2S, Fig. 3*C*). A similar trend was observed when the TIN2L concentration was increased (from 3.7% ± 1.7% of Type I at 25 nM TIN2L to 19.0% ± 10.6% at 100 nM TIN2L).

Consistent with observations from AFM imaging (Fig. 2), a significant population of traces showed bridging events involving multiple telomeric Cy3-DNA molecules (Fig. 4, *A* and *B*). By applying the Chung–Kennedy model (54, 55), we classified the traces based on the Cy3 signal intensity levels relative to the first baseline level in each trace to obtain the number of telomeric Cy3-DNA molecules bridged by proteins (Fig. 4*B*). This analysis showed that the percentages of complexes bridging multiple copies of the Cy3-DNA (n > 3) significantly increased with higher TIN2 concentrations (Fig. 4*C*). Specifically, while keeping TRF1 at a fixed concentration (100 nM), increasing TIN2S concentrations (25 nM, 50 nM, and 100 nM) led to a consistent increase in the percentages of telomeric Cy5-Cy3 DNA bridging events involving multiple Cy3-DNA molecules (n > 3). Overall, increasing the TIN2S concentration from 25 nM to 100 nM led to an approximately 4-fold increase (from 7.8% ± 2.1% to 34.7% ± 5.6%) in the percentage of bridging events involving multiple copies of telomeric Cy3-DNA molecules (n > 3, Fig. 4*C*). Under the same experimental conditions, increasing concentrations of TIN2L led to the same trend. The DNA-DNA bridging events involving multiple copies of telomeric Cy3-DNA molecules (n > 3) increased from 10.4% (±5.3%) at 25 nM TIN2L to 28.9% (±8.1%) at 100 nM TIN2L (Fig. 4*C*). Taken together, results from single-molecule TIRFM imaging experiments demonstrated that TIN2 increases the population of stable Type I complexes and thus the lifetimes of TRF1-mediated telomeric DNA-DNA bridging events. Furthermore, TRF1-TIN2 complexes are capable of promoting the bridging of multiple copies of telomeric DNA.

TRF1 loads TIN2 specifically onto the telomeric regions forming stable TRF1-TIN2 complexes

To further investigate the DNA-binding specificity and stability of TRF1-TIN2 complexes on longer telomeric DNA substrates, we applied the DNA tightrope assay. This assay (Experimental procedures) is based on oblique-angle fluorescence microscopy imaging of quantum dots (QDs)-labeled proteins on DNA anchored between silica beads (21, 56–58). DNA tightropes are formed by stretching DNA between poly-L-lysine-coated beads under hydrodynamic flow inside a flow cell. The defined spacing between specific DNA sequences and structures on DNA tightropes enables us to correlate DNA-binding events with specific DNA sequences or structures (21, 49–51, 59). Specifically, to study telomere-binding proteins, we ligated linear T270 fragments (LT270) to form DNA tightropes with telomeric regions (270 TTAGGG repeats) at defined spacing (Fig. 5, *A* and *B*). To monitor TRF1 and TIN2 (TIN2S or TIN2L) on DNA in real time, we conjugated His-tagged TRF1 to streptavidin-coated QDs (strep-QDs) and HA-tagged TIN2 to primary HA antibody-coated QDs (HA-Ab-QDs, Experimental procedures, Fig. 5*A*). QD labeling of TRF1 (21) or TIN2 does not significantly reduce telomeric DNA binding by TRF1 or TRF1-TIN2 (Fig. S10*A*). Strep-QD, Ab-QD, or TIN2-QDs without TRF1 did not nonspecifically bind to DNA tightropes (Data not shown). Experiments using combinations of TRF1 with HA-Ab-QDs or TIN2 with strep-QDs showed no significant cross talk between these two QD labeling strategies (Data not shown).

Consistent with results from our previous studies, TRF1 specifically binds to the telomeric region on DNA tightropes, with spacing between adjacent TRF1 on LT270 DNA tightropes matching the distance between telomeric regions (Fig. 5, *B* and *D*). To monitor the recruitment of TIN2 onto DNA tightropes by TRF1, we first added unlabeled TRF1 (10 nM) into the flow cell and incubate for 5 min, followed by the introduction of TIN2-QDs (either TIN2S or TIN2L, 10 nM) into the flow cell. Then the buffer flow was shut off to enable freely diffusing TIN2-QDs in solution to bind TRF1 on DNA tightropes. We observed long-lived TIN2S-QDs and TIN2L-QDs on LT270 DNA tightropes (Fig. 5*B*), with ~97% of TIN2-QDs remaining on DNA tightropes until the end of the observational windows (2 min: N = 1043; 5 min: N = 167).

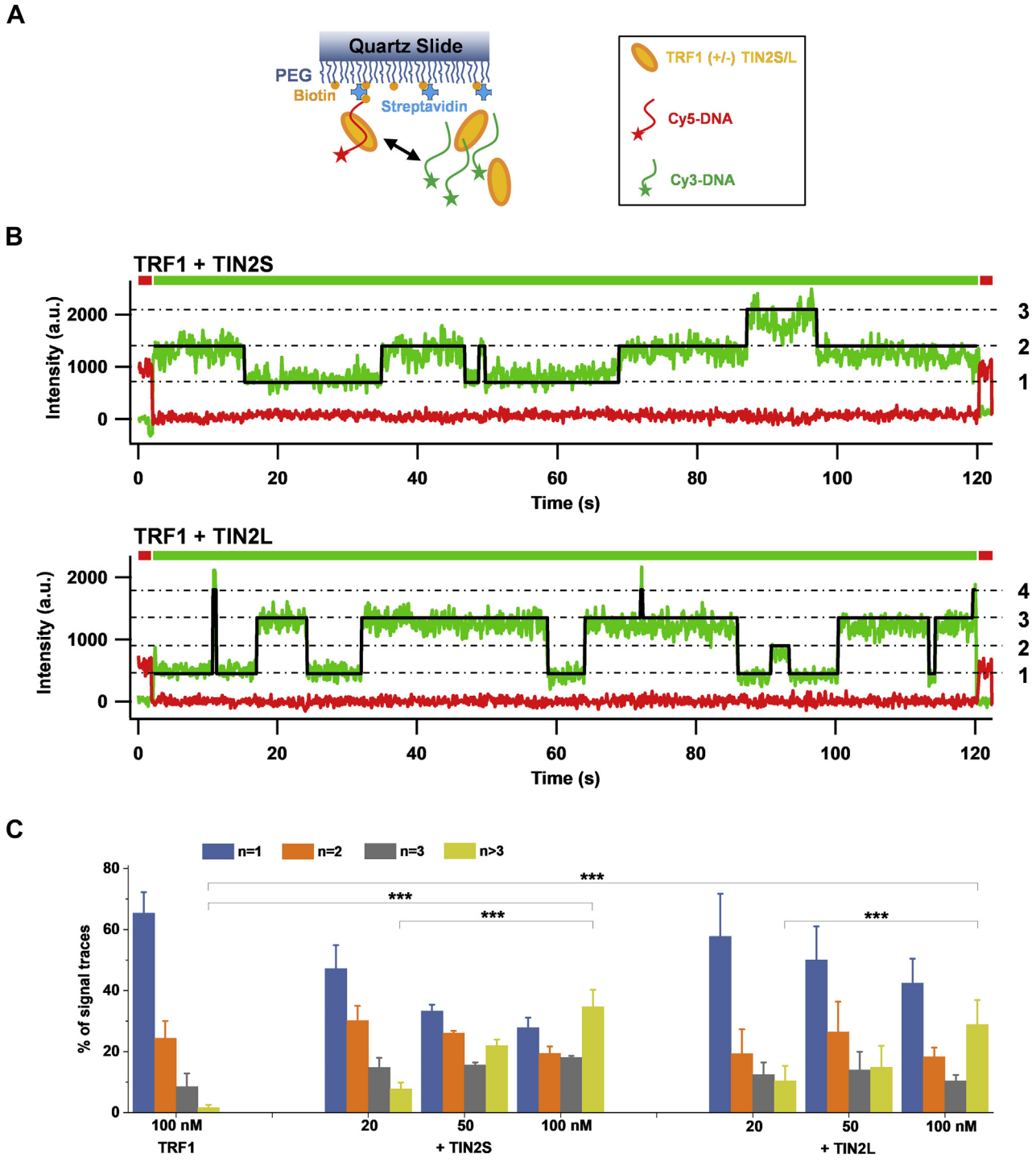

Figure 4. TRF1-TIN2 bridge multiple telomeric Cy3-DNA molecules to surface-anchored telomeric Cy5-DNA. *A*, schematics of multiple telomeric Cy3-DNA molecules being bridged to the surface-anchored telomeric Cy5-DNA by the TRF1-TIN2 complex. *B*, representative traces from TRIFM imaging showing multiple telomeric Cy3-DNA molecules being bridged by TRF1-TIN2S and TRF1-TIN2L to the surface-anchored telomeric Cy5-DNA. Dashed-dot lines indicate the number of telomeric Cy3-DNA molecules being bridged to the telomeric Cy5-DNA based on the fluorescence intensity of the Cy3 signals. The black lines are the fitting from the Chung–Kennedy model. *C*, percentages of telomeric Cy5-Cy3 DNA bridging events with 1, 2, 3, or greater than three Cy3-DNA molecules for TRF1 alone or TRF1 and increasing concentrations of TIN2S or TIN2L. The TRF1 concentration was kept constant (100 nM). Each data set was based on greater than 500 fluorescence traces collected from more than three independent experiments. Error bars: SEM. ***$p < 0.001$.

Furthermore, the majority of TIN2-QDs loaded by TRF1 (97%, N = 167) onto LT270 DNA tightropes were static throughout the observational window (5 min). To directly visualize the interaction between TRF1 and TIN2 on DNA tightropes, His-TRF1 and HA-TIN2 were differentially color labeled (Fig. S10*B*). Under the experimental condition tested (10 nM TRF1-QD, 10 nM TIN2-QD), 36.0% of the total protein-QDs on LT270 DNA tightropes were dual-color labeled, indicating colocalization (N = 339). Importantly, the pairwise distance between adjacent TIN2-QDs with unlabeled (Fig. 5*D*) or

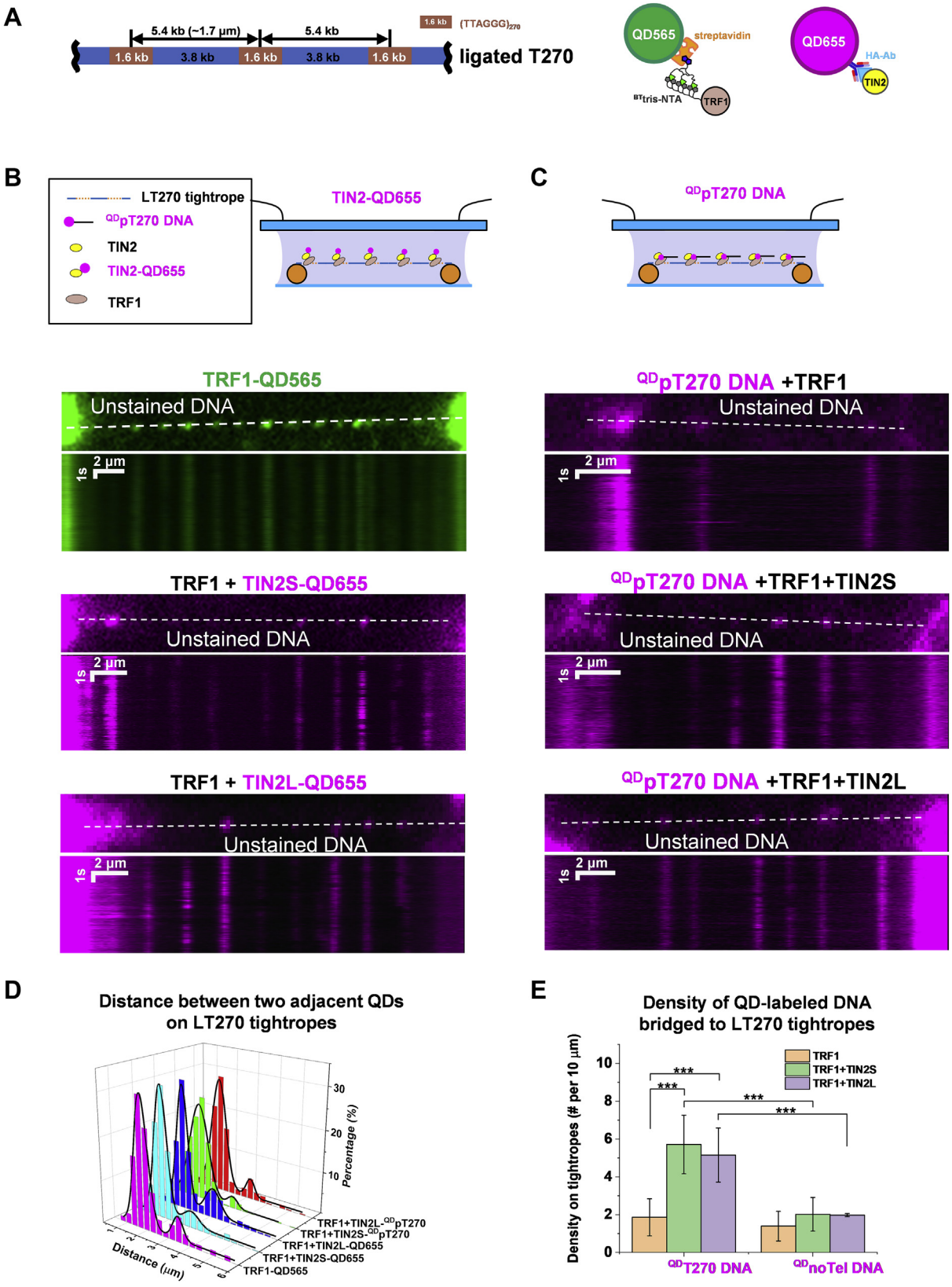

Figure 5. TIN2 is loaded specifically at telomeric regions by TRF1 and facilities TRF1-mediated telomeric double-stranded DNA-DNA bridging. *A*, schematics of the ligated T270 DNA substrate (*left panel*), and QD labeling schemes for TRF1 and TIN2 (*right panel*). His-tagged TRF1 was labeled with strep-QDs through the ^{Bt}tris-NTA compound. HA-tagged TIN2 was conjugated to HA-Ab-QDs. *B*, loading of TIN2 onto LT270 DNA tightropes by TRF1. Schematics of the experimental setup, and fluorescence images and kymographs of QD-labeled TRF1 alone, QD-labeled TIN2 on LT270 DNA tightropes in the presence of unlabeled TRF1. *C*, TRF1-TIN2 complex-mediated telomeric double-stranded DNA-DNA bridging. Schematics of the experimental setup and fluorescence images and kymographs of ^{QD}pT270 fragments on LT270 DNA tightropes in the presence of unlabeled TRF1, and TRF1-TIN2. *D*, the spacing between two adjacent QD-labeled TRF1, TIN2S, TIN2L, and ^{QD}pT270 on LT270 DNA tightropes, corresponding to experiments shown in *panels B* and *C*. Fitting the data

labeled TRF1 (Fig. S10*B*) was consistent with the expected spacing between telomeric regions on the LT270 DNA tightropes. In summary, results from the DNA tightrope assay showed that TIN2S and TIN2L are recruited by TRF1 specifically to the telomeric regions. Furthermore, TRF1-TIN2 form stable and long-lasting complexes on telomeric DNA.

TIN2S and TIN2L promote stable bridging of long telomeric DNA from solution to DNA tightropes

Having established that TRF1 loads TIN2 specifically at telomeric regions on DNA tightropes, we further tested whether TIN2 facilitates TRF1-mediated telomeric DNA-DNA bridging. For these experiments, the telomeric DNA strands anchored in place were LT270 DNA tightropes between micron-sized silica beads. The free DNA strands introduced into the flow cell were biotinylated double-stranded T270 fragments (270 TTAGG repeats without the flanking nontelomeric regions, pT270) or the control nontelomeric DNA (noTel, Experimental procedures, Fig. 5*C*). To visualize the pT270 DNA and noTel, we labeled the DNA strands with red (655 nm) strep-QDs. AFM imaging validated that 60.7% (±3.1%) of the pT270 and 67.7% (±6.7%) of the noTel DNA strands were labeled with strep-QDs (Fig. S11). With QD-labeled linear pT270 DNA (^{QD}pT270) alone, or ^{QD}pT270 DNA along with TIN2S or TIN2L in the flow cell, we did not observe any ^{QD}pT270 signals on LT270 DNA tightropes. Thus, we concluded that, in this experimental setup, since ^{QD}pT270 does not nonspecifically pair with DNA tightropes, localization of QD signals on DNA tightropes would provide a direct readout of bridging of the linear pT270 DNA to DNA tightropes by proteins.

To assess whether or not TIN2 facilitates TRF1-mediated DNA-DNA bridging, we added unlabeled TRF1 (10 nM) without or with TIN2 (TIN2S or TIN2L, 10 nM) into the flow cell and incubated for 5 min to allow proteins binding to LT270 DNA tightropes. Then we introduced ^{QD}pT270 (5 nM) along with additional TRF1 (10 nM), either without or with TIN2 (10 nM, Fig. 5*C*). While ^{QD}pT270 DNA signals on LT270 DNA tightropes were sparse when only TRF1 was present (1.86 ± 0.98 QD signals per 10 μm of DNA, Fig. 5, *C* and *E*), we observed significantly higher densities of ^{QD}pT270 signals (per 10 μm of DNA length) on LT270 DNA tightropes when both TRF1 and TIN2 were present (5.7 ± 1.6 for TIN2S and 5.2 ± 1.4 for TIN2L, Fig. 5, *C* and *E*). Furthermore, with control nontelomeric DNA (noTel), the density of ^{QD}noTel bridged to LT270 DNA tightropes (per 10 μm DNA length) was significantly lower (1.39 ± 0.78 for TRF1, 2.02 ± 0.89 for TRF1-TIN2S, and 1.98 ± 0.08 for TRF1-TIN2L, Fig. 5*E*). The linear ^{QD}pT270 DNA bridged onto DNA tightropes was long-lasting, with 95.5% (±3.1%, N = 438) of the ^{QD}pT270 DNA molecules staying on DNA tightropes until the end of the 5-min observational windows. Furthermore, the spacing between two adjacent ^{QD}pT270 signals mediated by TRF1-TIN2S and TRF2-TIN2L on the DNA tightropes was consistent with the distance between telomeric regions (Fig. 5*D*). Considering an average center-to-center spacing of 1.5 μm between $(TTAGGG)_{270}$ regions on DNA tightropes, six $(TTAGGG)_{270}$ regions are expected for every 10 μm of DNA tightropes. An occupancy of ~5 ^{QD}pT270 signals per 10 μm of DNA tightropes suggested that, in the presence of TRF1-TIN2, the majority of $(TTAGGG)_{270}$ regions contained protein bridged ^{QD}pT270 DNA. Furthermore, TRF1-TIN2 was capable of mediating the bridging of short $(TTAGGG)_6$ dsDNA to LT270 DNA tightropes (Fig. S12).

To further confirm that TIN2 was present in the DNA-DNA bridging complex, we differentially labeled HA-tagged TIN2 and pT270 DNA fragments with HA-Ab-QDs (red) and strep-QDs (green), respectively (Fig. S13*A*). The majority of ^{QD}pT270 (~87%, N = 28) bridged to LT270 DNA tightropes was colocalized with TIN2 (Fig. S13*B*). Taken together, these results from the DNA tightrope assay established that TIN2 facilitates stable TRF1-mediated bridging of physiologically relevant long telomeric DNA molecules.

TIN2 protects TRF1-mediated DNA-DNA bridging in the presence of Tankyrase 1

Telomeric DNA binding by TRF1 is regulated by Tankyrase 1, a member of the poly(ADP-ribose) polymerase (PARP) family of proteins that directly interacts with the acidic domain of TRF1 (37, 60). Poly(ADP-Ribosyl)lation (PARylation) of TRF1 inhibits telomeric DNA binding by TRF1 *in vitro* (37). Consistent with these previous observations, EMSA revealed that Tankyrase 1 reduced the formation of TRF1-DNA complexes (compare lanes 2, 3, and 4 in Fig. S14). Consistent with results from the EMSAs, preincubation of TRF1 with Tankyrase 1 and NAD^+ reduced the loading of QD-labeled TRF1 on LT270 DNA tightropes (Fig. S15, *A* and *C*). Previous work showed that TIN2-TRF1-Tankyrase 1 form a ternary complex, and TIN2 blocks the modification of TRF1 by Tankyrase 1 *in vitro* (61). Preincubation of TRF1 and TIN2S protected TRF1 telomeric DNA binding (compare lanes 6 and 7 in Fig. S14).

To further investigate whether TIN2 protects TRF1-mediated DNA-DNA bridging from Tankyrase 1, we monitored the bridging of ^{QD}pT270 DNA on LT270 DNA tightropes in the same flow chamber under different conditions (Fig. 6*A*, top panel). We first established that the large majority of ^{QD}pT270 DNA (>90%) bridged onto LT270 DNA tightropes by TRF1-TIN2 could be removed by extensive washing with the imaging buffer (Fig. 6*A*, bottom panel). Thus, we designed four sequential experiments using the same flow chamber in the following sequence, with washing steps

with double Gaussian functions ($R^2 > 0.92$) for protein-QD signals (related to *panel B*) shows peaks centered at 1.63 μm and 3.29 μm (N = 185) for TRF1-QDs, 1.60 μm and 3.02 μm for TRF1-TIN2S-QDs (N = 538), and 1.63 μm and 3.09 μm for TRF1-TIN2L-QDs (N = 288). Fitting the data with double Gaussian functions ($R^2 > 0.86$) for ^{QD}pT270 signals (related to *panel C*) shows peaks centered at 1.49 μm and 3.13 μm TRF1-TIN2S (N = 321), and 1.57 μm and 3.14 μm for TRF1-TIN2L (N = 318). *E*, the densities of QD-labeled pT270 and noTel DNA on the LT270 DNA tightropes (per 10 μm DNA length), mediated by TRF1 alone (1.86 ± 0.98 on pT270: N = 132; 1.39 ± 0.78 on noTel: N = 50), TRF1-TIN2S (5.7 ± 1.6 on pT270: N = 364; 2.02 ± 0.89 on noTel: N = 98), and TRF1-TIN2L (5.2 ± 1.4 on pT270: N = 388; 1.98 ± 0.08 on noTel: N = 105). ***$p < 0.001$.

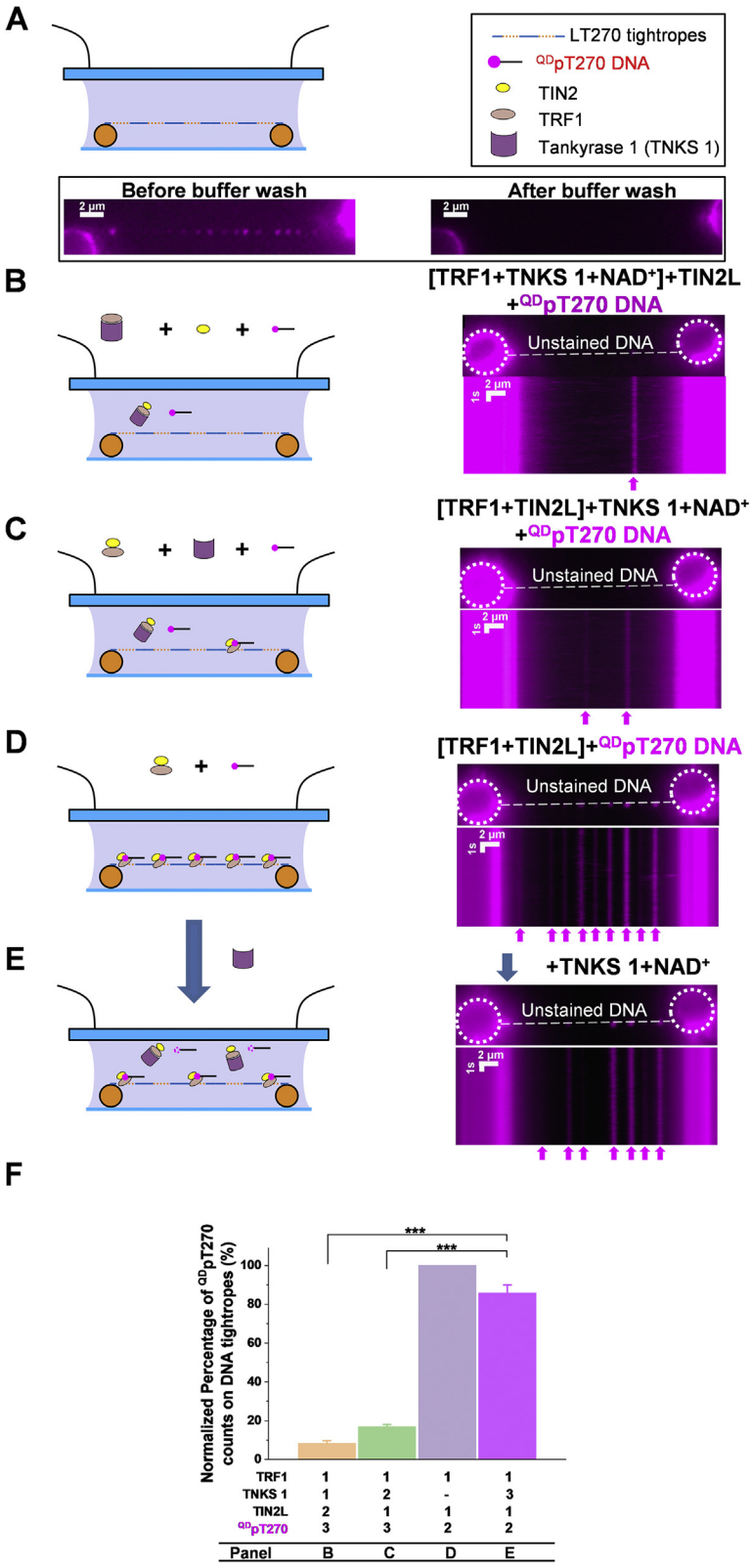

Figure 6. TIN2 protects TRF1-mediated DNA-DNA bridging in the presence of Tankyrase 1 and NAD$^+$. *A*, schematics of the DNA tightrope assay and reagents (*top panel*), and the control experiment showing the efficiency of removing TRF1-TIN2 bridged ^{QD}pT270 DNA fragments from tightropes (*bottom panel*). *B–E*, schematics (*left panels*) and examples of fluorescence images and kymographs (*right panels*) from using the following protein solutions mixed with the ^{QD}pT270 DNA (200 nM). *B*, TRF1 was preincubated with Tankyrase 1 (TNKS 1) and NAD$^+$ before the addition of TIN2L. *C*, TRF1 and TIN2L were preincubated together before the addition of Tankyrase 1 and NAD$^+$. *D*, TRF1 and TIN2L were incubated together without Tankyrase 1 and NAD$^+$. *E*, after recording the TRF1+TIN2L+ ^{QD}pT270 experiments (*D*) and flushing the flow chamber with the imaging buffer, TNKS 1 and NAD$^+$ were introduced into the flow chamber. The arrows at the bottom of each kymograph point to the QD-labeled ^{QD}pT270 DNA bridged onto LT270 DNA tightropes. *F*, quantification of the density of ^{QD}pT270 DNA bridged to LT270 DNA tightropes under the conditions showed in *panels B–E*. The percentage was normalized to the condition in D (TRF1+TIN2L, N = 521 ^{QD}pT270 signals on tightropes). The numbers in the *x*-axis label indicate protein and DNA addition sequence. ***$p < 0.001$.

to remove previously bound protein-^{QD}pT270 complexes, followed by the introduction of new protein-^{QD}pT270 mixtures before taking videos. This experimental design allowed us to directly compare protein-mediated bridging of ^{QD}pT270 DNA fragments onto the same sets of LT270 DNA tightropes without or with Tankyrase 1 and NAD^+ (150 μg/ml Tankyrase 1, 120 μM NAD^+, Fig. 6, *B–E*). We first premixed TRF1 (200 nM), Tankyrase 1, and NAD^+ followed by adding TIN2L (200 nM, Fig. 6*B*). Next, after washing the flow chamber, we introduced a second protein mixture containing TRF1 (200 nM) preincubated with TIN2L (200 nM) before the addition of Tankyrase I and NAD^+ (Fig. 6*C*). After these two experimental conditions containing Tankyrase 1 and washing the flow chamber, we introduced TRF1 (200 nM) and TIN2L (200 nM) into the flow chamber along with ^{QD}T270 DNA fragments to benchmark the level of ^{QD}pT270 DNA bridged onto LT270 DNA tightropes without Tankyrase 1 and NAD^+ (Fig. 6*D*). Finally, we introduced Tankyrase 1 and NAD^+ into the flow chamber to monitor the dismantling of TRF1-TIN2L-mediated bridging of ^{QD}pT270 DNA by Tankyrase 1 (Fig. 6*E*). To monitor the bridging of ^{QD}pT270 to DNA tightropes, each protein mixture was incubated with ^{QD}pT270 DNA fragments (200 nM) for 10 min and diluted 50 times in the imaging buffer before being sequentially introduced into the flow chamber containing LT270 DNA tightropes. The direct comparison from this series of experiments revealed that after TRF1-TIN2L-mediated DNA-DNA bridging was formed (^{QD}pT270 on DNA tightropes normalized at 100%, Fig. 6*D*), the introduction of Tankyrase 1 and NAD^+ reduced the ^{QD}pT270 DNA bridging events on L270 DNA tightropes (85.8% ± 4.1%, Fig. 6, *E* and *F*). Importantly, this level of DNA-DNA bridging events was significantly higher than when TRF1-TIN2L-Tankyrase 1 were preincubated together before the inclusion of ^{QD}T270 DNA fragments (16.9% ± 1.1%, Fig. 6, *C*, *E*, and F). Furthermore, inhibition of TRF1-TIN2-mediated DNA-DNA bridging on DNA tightropes depends on the presence of both Tankyrase 1 and NAD^+ (Fig. S15, *B* and *C*). In summary, these results demonstrated that TIN2 in the TRF1-TIN2 DNA-DNA bridging complex is more efficient in protecting TRF1 from Tankyrase 1 modification than when TRF1-TIN2 are free in solution.

TPP1 inhibits TRF1-TIN2-mediated telomeric double-stranded DNA-DNA bridging

A previous single-molecule study tracking the full shelterin complex by fluorescently labeling telomeric ssDNA bound to POT1 demonstrated that shelterin forms individual complexes and does not promote DNA-DNA bridging (62). Our DNA tightrope assay and AFM imaging demonstrate that TIN2 facilitates TRF1-mediated DNA-DNA bridging (Fig. 2 and 4–6). However, whether or not other shelterin components, such as TPP1, influence DNA-DNA bridging by TRF1-TIN2 is unclear. To directly address this question, we purified Hexahistidine SUMO-tagged (amino acids 89–334, His-SUMO-TPP1N, Fig. S16*A*), as well as untagged N-terminal domain of TPP1 (Experimental procedures). We confirmed that His-SUMO-TPP1N interacts with POT1 to stimulate telomerase processivity (Fig. S16, *B* and *C*) and does not bind to DNA by itself (Fig. S16*D*). AFM imaging of the linear T270 DNA (5 nM) with TRF1 (300 nM), TIN2L (300 nM), and His-SUMO-TPP1N (300 nM) revealed significantly ($p < 0.05$) fewer DNA molecules (20.4% ± 5.8%, N = 836) in protein–DNA clusters containing more than two T270 fragments (Fig. 7*A*), compared with reactions lacking His-SUMO-TPP1N (42.5% ± 5.1%, Fig. 2*D*). To visualize TPP1N on DNA tightropes, we conjugated His-SUMO-TPP1N to secondary antibody-coated QDs using the antibody sandwich method (^{QD}TPP1N, Fig. 7*B*). We then directly compared the DNA-DNA bridging efficiency by introducing into the flow cell unlabeled TRF1, TIN2L, SUMO antibody, green secondary-antibody-coated QDs, and red QD-labeled linear pT270 fragments (^{QD}pT270) either without or with His-SUMO-TPP1N (10 nM each component, Fig. 7*B*). Without TPP1N, no significant green QD signals were observed on the LT270 DNA tightropes. This result demonstrates that the SUMO antibody and secondary antibody-coated QDs did not bind nonspecifically to TRF1, TIN2, or DNA tightropes. In contrast, in the presence of TRF1, TIN2L, and His-SUMO-TPP1N, we observed green QDs marking TPP1N on LT270 DNA tightropes with a density of 3.7 QD signals per 10 μm of DNA (Fig. 7, *B* and *C*). This result demonstrates that TRF1-TIN2L recruited TPP1N to LT270 DNA tightropes. Strikingly, when TRF1-TIN2L-TPP1N were present in the flow cell, the density of ^{QD}pT270 bridged onto LT270 DNA tightropes (1.31 ± 0.75/10 μm) was significantly lower compared with conditions with TRF1-TIN2L but lacking TPP1N (5.65 ± 0.33/10 μm, Fig. 7, *B* and *C*).

Consistent with results from the DNA tightrope assay, EMSA showed that with fixed TRF1 and TIN2L concentrations (200 nM each) and increasing concentrations of His-SUMO-TPP1N (50, 100, and 200 nM), the higher-order protein–DNA complexes were reduced (complex III, Figs. 7*D* and S16*E*), while the overall DNA binding remained the same. The same putative interaction between TIN2L and TPP1N was indicated when HA-TIN2L immobilized onto protein G beads pulled His-SUMO-TPP1N and untagged TPP1N out of solution (Fig. S17, *A* and *B*. Furthermore, the identity of TPP1N pulled-down by TIN2L was confirmed using mass spectrometry. These results established that TPP1N directly interacts with TIN2L in solution without DNA (Fig. S17). Thus, taken these results together, we conclude that TPP1N interacts with TIN2L *in vitro* and inhibits the TRF1-TIN2L mediated DNA-DNA bridging without significantly affecting the direct binding of TRF1-TIN2L to telomeric DNA.

Discussion

Despite the central role that TIN2 plays in telomere maintenance, the mechanism underlying its function had been largely unknown. Our results from three single-molecule imaging platforms provide new mechanistic insight supporting the notion that TIN2 facilitates TRF1-mediate DNA compaction and DNA-DNA bridging through several key

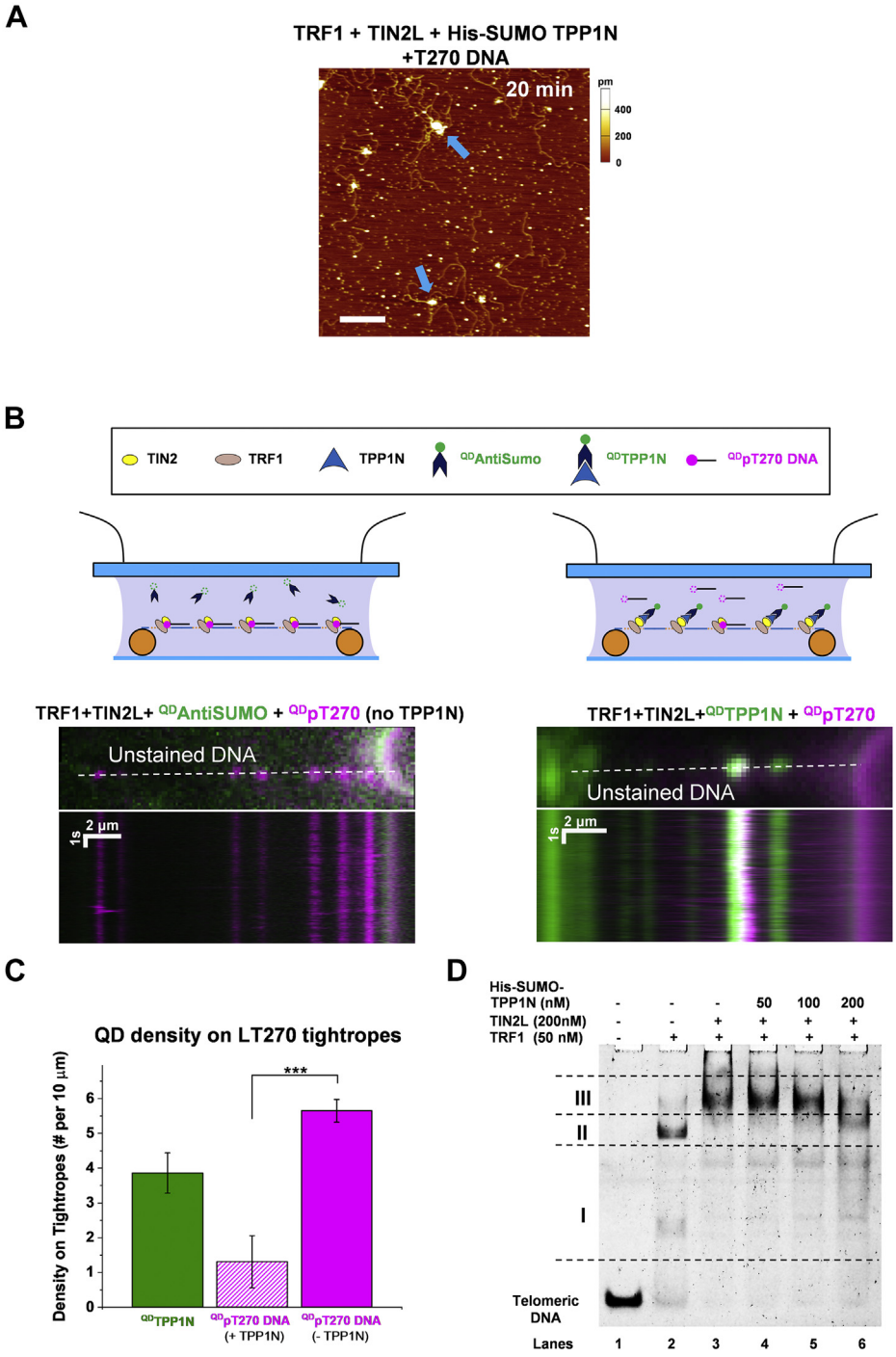

Figure 7. TPP1N inhibits TRF1-TIN2L-mediated DNA-DNA bridging. *A*, an AFM image of the linear T270 fragment (5.4 kb, 5 nM) in the presence of TRF1 (300 nM), TIN2L (300 nM), and His-SUMO-TPP1N (300 nM). The sample was incubated at room temperature for 20 min before being diluted 20-fold in the buffer and deposited onto a mica surface. XY scale bar: 500 nm. *B*, comparison of the efficiency in bridging red QD-labeled pT270 DNA to LT270 DNA tightropes in the presence of TRF1, TIN2L, either without (*left panel*), or with His-SUMO-TPP1N (labeled with green QDs, *right panels*). Schematics depicting the experimental setup (*top panels*) and fluorescence images and kymographs (*bottom panels*). Unlabeled TRF1, TIN2L, SUMO antibody, secondary-antibody-coated QDs, and ^{QD}pT270 DNA fragments were present in both experimental conditions. *C*, quantification of the density of ^{QD}TPP1N on L270 DNA tightropes (per 10 μm DNA length) in the presence of TRF1-TIN2L (3.86 ± 0.58, N = 108) and of ^{QD}pT270 on LT270 DNA tightropes in the presence of TRF1, TIN2L, ^{QD}AntiSUMO either with (1.31 ± 0.75, N = 34 QDs) or without His-SUMO-TPP1N (5.66 ± 0.33, N = 152 QDs). ***$p < 0.001$. *D*, EMSA showing mobility shift induced by the binding of TRF1, TRF1-TIN2L and increasing concentrations of His-SUMO-TPP1N. DNA substrate: Alexa 488-labeled dsDNA containing three TTAGGG repeats (5 nM).

observations. We discovered that, in the presence of both TRF1 and TIN2, large clusters of protein complexes (AFM volume > 500 nm^3) formed at telomeric DNA regions and shortened the lengths of individual T270 DNA molecules. AFM imaging revealed the time-dependent formation of clusters of telomeric DNA fragments bridged by multiprotein TRF1-TIN2 complexes. TIRFM tracking of colocalization of surface-anchored telomeric Cy5-DNA and Cy3-DNA from

solution showed that *trans*-interactions (DNA-DNA bridging) were telomeric sequence- and TIN2 concentration-dependent. Increasing TIN2 concentrations led to larger percentages of stable telomeric DNA-DNA bridging events (>2 min) and multiple telomeric DNA fragments (n > 3) bridged by proteins. With longer telomeric DNA length (270 TTAGGG repeats), the majority (approximately five out of six) of the telomeric regions contained telomeric pT270 fragments bridged to DNA tightropes. The DNA-DNA bridging events (*trans*-interactions) on LT270 DNA tightropes mediated by TRF1-TIN2 were stable and lasted for more than 5 min. These results support the notion that multiprotein TRF1-TIN2 complexes facilitate both *cis*-interactions on the same telomeric DNA and *trans*-interactions by stabilizing the bridging of telomeric DNA. Finally, we observed that TPP1N inhibits TRF1-TIN2L-mediated DNA-DNA bridging.

The current literature remains inconclusive regarding the activities of specific shelterin proteins in the compaction of double-stranded telomeric DNA. Previous EM and AFM studies revealed that TRF1 promotes telomeric DNA-DNA pairing and TRF2 compacts telomeric DNA (14, 17, 20, 22, 47, 49). These results suggested that shelterin proteins might play keys roles in modulating double-stranded telomeric DNA configurations. Furthermore, Bandaria *et al.* measured the telomere size using superresolution photoactivated localization microscopy (PALM) imaging of mEos2-labeled shelterin proteins and fluorescence *in situ* hybridization–stochastic optical construction microscopy (FISH-STORM) imaging (63). They suggested that telomeres form compact globular structures through a dense network of specific protein–protein and protein–DNA interactions. Based on this previous study, TRF1, TRF2, and TIN2 are the main contributors to the telomere compaction, with depletion of TRF1 and TIN2 using siRNA leading to a 8-fold and 4-fold increase in the telomere volume, respectively (63). Based on these observations, shelterin-mediated telomere compaction was proposed to be a general mechanism for suppressing DDR pathways at telomeres. However, two recent studies using STORM imaging of telomeres marked with telomeric FISH probes suggested that telomeric compaction upon shelterin removal is either minor or only affects small subsets of telomeres (64, 65). In addition, the telomeres showing DDR do not significantly differ in size compared with the ones that are DDR-negative (65). Consistent with these two later studies, single-molecule fluorescence imaging of shelterin proteins on DNA curtains suggested that shelterin binds to telomere DNA as individual complexes (62). In this study, shelterin protein-mediated DNA-DNA bridging was assessed by the retention of the single-tethered DNA onto the double-tethered DNA curtains after buffer flow was turned off. Through using this imaging platform, the authors observed that when shelterin proteins were present, single- and double-tethered DNA molecules separated immediately after buffer flow was switched off. Based on these observations, the authors concluded that shelterin proteins do not promote strong *trans*-interactions.

The discrepancy between results from this previous single-molecule study and our current one could stem from three sources. The first potential source is that the length of the telomeric DNA sequences here was nine times larger than what was used in the prior studies (32 repeats in the previous study *versus* 270 repeats in our current study). The second potential source of the discrepancy is that our experiments provide freedom of 3D diffusion for at least one telomeric DNA strand that enables the search process. This is critical for protein-mediated DNA-DNA bridging. In the DNA curtain experiment, under flow-stretched configuration, the single-tethered molecules might not be able to fully search in 3D space to pair with the double-tethered DNA. In comparison, in our DNA tightrope assay and TIRFM colocalization setup, the ^{QD}pT270 DNA-TRF1-TIN2 and Cy3-DNA-TRF1-TIN2 complexes introduced into the flow cell were free to diffuse in 3D. These experimental conditions enabled 3D diffusion to facilitate the bridging of two DNA molecules. The third potential source of discrepancy between our results and prior studies are the distinct functions of TRF1-TIN2 subcomplexes and the full shelterin complexes. In the DNA curtain experiments, the focus was the DNA binding dynamics of the full shelterin complexes marked with a fluorescent telomeric ssDNA bound to POT1 (62). Given that TRF1 and TIN2 are approximately ten times more abundant than TPP1, *in vivo* the majority of TRF1-TIN2 on telomeres lack TPP1 (44). Combining our results with this previous single-molecule study using DNA curtains strongly suggests that shelterin assembly at telomeres is heterogeneous with different subcomplexes and full complexes playing distinct roles in telomere maintenance.

Our results are consistent with a model in which multiple factors contribute to the compaction of telomeres. Compaction of telomeres by additional factors such as nucleosomes or other proteins that remain unidentified could minimize the decompaction effect observed upon shelterin removal. Furthermore, the results from our study are consistent with the critical role that TIN2 plays in TRF1-TIN2-SA1-mediated sister telomere cohesion that is largely cohesin-ring independent (8, 36, 66). While siRNA depletion of TRF1 does not significantly affect sister telomere cohesion, depletion of TIN2 leads to a sister cohesion defect. Previously, we reported that SA1 and TRF1 together promote telomeric DNA-DNA pairing tracks (49). The results from AFM, TIRFM imaging, and the DNA tightrope assay reported in this study demonstrate that TIN2 further facilitates TRF1-mediated *trans*-interactions between different telomeric DNA fragments. Furthermore, TIN2 is more efficient in protecting TRF1 from Tankyrase 1 modification when present in the large multiprotein TRF1-TIN2-DNA complexes than when TRF1 is free in solution. Based on results from our current study and previous ones (8, 36, 49, 66), we propose that TIN2 is a key architectural protein that links a telomeric DNA-binding protein (TRF1) and a cohesin subunit (SA1) to promote *trans*-interactions that are essential for sister telomere cohesion.

Previously, it was shown that the C-terminal domain TPP1 mediates the interaction between TPP1 and TIN2 (25, 27, 67). In our study, complementary results from the DNA tightropes assay, EMSA, and protein G pull-down using purified proteins

showed that the N-terminal domain of TPP1 (amino acids 89–334) directly interacts with TIN2L *in vitro* and disrupts multiprotein TRF1-TIN2-mediated DNA-DNA bridging.

It is worth noting that our single-molecule experiments demonstrate that both TIN2S and TIN2L isoforms show similar activities in promoting TRF1-mediated DNA compaction and DNA-DNA bridging. Defect observed with TRF1-TIN2S-13 suggested that the N-terminal domain of TIN2 plays a key role in facilitating TRF1-mediated DNA-DNA bridging. Notably, a recent study demonstrated that TIN2L, but not TIN2S, is phosphorylated by the casein kinase 2 (CK2) (68). TIN2L phosphorylation enhances its association with TRF2 *in vivo*, while TRF1 interacts more robustly with TIN2S than TIN2L in the cellular environment (68). To advance our understanding of the unique biological functions of each TIN2 isoform, future work is needed to uncover differences in their interactions with other protein partners.

Experimental Procedures

Protein purification

Recombinant N-terminal His_6-tagged TRF1 (from human) was purified using a baculovirus/insect cell expression system and an AKTA Explorer FPLC (GE Healthcare) as described in a previous study (69). N-terminal HA-tagged TIN2L (HA-TIN2L, 1–451 aa) and TIN2S (HA-TIN2S, 1–354 aa) were expressed in the Sf-900 insect cells using the pFastBac1 expression system (GenScript). HA-TIN2L and HA-TIN2S were purified using anti-HA resin and stored in a buffer containing 50 mM Tris-HCl (pH 7.5), 150 mM NaCl, 10% glycerol, 1% NP40, and 1 mM EDTA. The concentrations of TIN2 proteins were determined by the BCA protein assay with BSA as the standard (Thermo Fisher). The identities of purified HA-TIN2S and HA-TIN2L proteins were confirmed by the Western Blot analysis using the HA antibody (GenScript A00168), and MALDI-TOF mass spectrometry analysis (UNC-Chapel Hill Proteomics Center). GST-tagged TIN2S-13 was cloned into the pGEX vector, overexpressed in BL21(DE3) pLysS cells, and purified using GST beads according to standard protocol. His-tagged Tankyrase 1 (a gift from Susan Smith at NYU) was purified from Sf21 insect cells, as described previously (37).

Hexahistidine SUMO-tagged (amino acids 89–334, His-SUMO-TPP1N) and untagged (TPP1N) N-terminal TPP1 proteins were purified from soluble lysates of isopropyl β-d-thiogalactopyranoside (IPTG)-induced BL21(DE3) pLysS cells (Promega) using nickel agarose chromatography and size-exclusion chromatography (SEC) based on protocols described previously (70–72). Specifically, after incubating the cell lysate with Ni-NTA agarose beads (Qiagen), the protein was eluted from the beads with 250 mM imidazole, and fractions containing TPP1N were concentrated and buffers exchanged (25 mM Tris pH 7.5, 150 mM NaCl, 5% glycerol) using a Centricon-10 device (Amicon). The sample was incubated with SUMO (Ulp1) protease (Invitrogen) overnight at 4 °C with rotation at 20 rpm to cleave the tag. For the uncleaved TPP1N (His-SUMO-TPP1N) protein, this step was omitted. The sample was then loaded onto a Superdex 75 Increase 10/200 GL column (GE Healthcare) equilibrated with 25 mM Tris pH 7.5, 150 mM NaCl, 5 mM DTT, 5% glycerol, and protease inhibitors. Eluted fractions containing TPP1N were collected, pooled, and concentrated. Protein concentration was determined by Bradford Assay (Bio-Rad), and purity was determined by SDS-PAGE and Coomassie staining.

Size-exclusion chromatography

SEC was carried out using the Superdex 200 10/300 GL column (GE Healthcare) connected to a BioLogic DuoFlow chromatography system (Bio-Rad). The SEC runs were conducted at 4 °C and a flow rate of 0.25 ml/min using a buffer containing 20 mM HEPES (pH 7.9), 100 mM NaCl, 0.3 mM $MgCl_2$, 1 mM EDTA, and 0.5 mM DTT.

DNA substrates

The plasmid (5.4 kb, T270) containing two $(TTAGGG)_{135}$ regions linked by 23-bp nontelomeric sequences was purchased from Addgene (pSXneo(T2AG3), #12403) (73). For AFM imaging, the T270 plasmid was digested by HpaI at 37 °C for 4 h in the CutSmart buffer (New England BioLabs) to place the $(TTAGGG)_{270}$ at the middle region of the linearized substrate. In order to generate longer DNA substrates for fluorescence imaging, the linearized T270 was ligated using the Quick Ligation Kit (New England BioLabs) at room temperature for 1 h followed by additional incubation at 4 °C for overnight. Ligated T270 was purified to remove ligase by phenol-chloroform extraction using the Phase Lock Gel (Quantabio). The biotinylated T270 substrate (pT270) and control DNA (noTel) were generated through biotinylation of the gel-purified T270 fragment containing the $(TTAGGG)_{270}$ region (pT270, 1.6 kb) or control nontelomeric DNA (noTel, 4.1 kb) using the 5′ EndTag Labeling DNA/RNA Kit (Vector Laboratories). The biotinylation of the pT270 and noTel fragments was verified using AFM imaging of DNA samples in the presence of streptavidin-coated quantum dots (strep-QDs, Invitrogen). All oligos were purchased from IDT. Cy5/biotinylated DNA (69 bp) with six TTAGGG repeats used for the single-molecule TIRF experiments was generated by annealing the Cy5-labeled oligo (Cy5-5′TCTGTAGTGTA *TTAGGGTTAGGGTTAGGGTTAGGGTTAGGGTTAGGG*ATGTAGGTATGTCACAGCATGA3′) and complementary biotin-labeled oligo (biotin-5′TCATGCTGTGACATACCTACAT *CCCTAACCCTAACCCTAACCCTAACCCTAACCCTAA*TACACTACAGA3′). Cy3-DNA without biotin (59 bp) was prepared by annealing Cy3-labeled oligo (Cy3-5′ACATACCTACATC*CCCTAA CCCTAACCCTAACCCTAACCCTAACCCTAA*TACACTACAGA3′), and complementary oligo (5′TCTGTAGTGTA*TTAGGGTTAGGGTTAGGGTTAGGGTTAGGGTTAGGG*ATGTAGGTATGT3′). The telomeric DNA substrate used for electrophoresis mobility shift assays (EMSAs) was constructed by annealing a 5′-Alexa488-labeled oligo (5′*TTAGGGTTAGGGTTAGGG*ATGTCCAGCAAGCCAGAATTCGGCAGCGTA3′) with its complementary oligo.

Electrophoresis mobility shift assays (EMSAs)

Protein–DNA binding reactions were carried out in a buffer containing 20 mM HEPES (pH 7.9), 100 mM NaCl, 1 mM EDTA, 0.5 mM DTT, 0.25% NP-40, and 5% glycerol. The samples were incubated at room temperature for 20 min and loaded onto a 5% 29:1 (bisacrylamide:acrylamide) native gel. Electrophoresis was carried out at 150 V for 40 min in 1× TBE buffer at 4 °C. The gel was visualized using a Typhoon Phosphorimager (FLA 7000).

Protein-quantum dot conjugation

Green (565 nm) strep-QDs (Life Technologies) were conjugated to N-terminal His_6-tagged TRF1 proteins through the multivalent tris-nitrilotriacetic acid chelator (^{BT}tris-NTA) as previously reported (21). The primary HA antibody (Covance, catalogue number: MMS-101P) was conjugated to red (655 nm) QDs using the SiteClick QD antibody labeling kit (Life Technologies) according to the manufacturer's standard protocols. The final concentration of HA-Ab-QDs was measured on NanoDrop (Thermo Fisher). HA-Ab-QDs were then conjugated to HA-tagged TIN2S or TIN2L by incubation at a 1: 1 ratio for 20 min at room temperature. His-SUMO-TPP1N was conjugated to the secondary antibody-coated QDs by incubating TPP1N, the SUMO antibody (sc-137158 Smt3 antibody E-1, Santa Cruz Biotechnology), and secondary-antibody-coated QDs at 1:1:1 ratio and 1 μM final concentration each at room temperature for 20 min.

Atomic force microscopy (AFM) imaging

TRF1 and TIN2 were incubated in a buffer containing 20 mM HEPES (pH 7.9), 100 mM NaCl and 1 mM EDTA at a 1:1 ratio (300 nM: 300 nM). After 10 min of incubation at room temperature, linearized telomeric T270 DNA (5.4 kb, 5 nM) or control DNA (noTel DNA, 4.1 kb) was added into the protein mixture and incubated for time durations as indicated in the figures. The sample was diluted 10-fold using the AFM imaging buffer (25 mM HEPES, pH 7.5, 25 mM NaOAc, and 10 mM $Mg(OAc)_2$) before being deposited onto a freshly peeled mica surface (SPI supplies).

The DNA tightrope assay

The oblique angle TIRFM-based DNA tightrope assay was described previously (49, 50, 56–58). Briefly, we immobilized poly-L-lysine (2.5 mg/ml, M.W.>30,000 KDa, Wako Chemicals) treated silica beads onto a PEGlyated coverslip surface and then introduced ligated DNA substrates into the flow cell using a syringe pump at a flow rate of 300 μl/min to stretch the DNA between treated beads. All protein-QD samples were diluted 100-fold using the imaging buffer (20 mM HEPES, pH 7.9, 100 mM NaCl, 0.3 mM $MgCl_2$, 1 mM EDTA, 0.5 mM DTT, and 1 mg/ml BSA) to a final concentration of 10 nM proteins in the imaging chamber. Additional 10-min incubation was taken before video recording. To prevent nonspecific binding, 1× Blocking Reagent (Sigma, catalog number 11096176001) was used in the imaging buffer. For experiments investigating the impact of Tankyrase 1 on the efficiency TRF1-TIN2-mediated bridging of QD-labeled linear telomeric pT270 DNA to LT270 DNA tightropes, we carried out a series of four sequential experiments in the same flow chambers. After videos were taken under each condition, the flow chamber was flushed with the imaging buffer (200 μl, ~6× of the flow chamber volumes) to set up for the next experiment. We confirmed that greater than 90% of the ^{QD}pT270 fragments on DNA tightropes were washed off under this condition. The four sequential experiments were designed as follows: (1) TRF1 (200 nM) was preincubated with Tankyrase 1 (150 μg/ml) and NAD^+ (120 μM, MilliporeSigma, catalog number 481911) for 30 min before the addition of TIN2L (200 nM) and further incubation for 20 min; (2) TRF1 (200 nM) and TIN2L (200 nM) were preincubated together for 20 min before the addition of Tankyrase 1 (150 μg/ml) and NAD^+ (120 μM) followed by further incubation for 30 min; (3) TRF1 (200 nM) and TIN2L (200 nM) were incubated together for 20 min without Tankyrase 1 and NAD^+. For all three experiments, the protein solutions were mixed with 200 nM QD-labeled pT270 DNA and diluted 50-fold using the imaging buffer before being introduced into the flow chamber and further incubated in the flow chamber for 10 min before video recording. After the third experiment and flushing of the flow chamber, Tankyrase 1 (150 μg/ml) and NAD^+ (120 μM) were introduced into the flow chamber and incubated for 30 min with the DNA tightropes to monitor the disassembly of the ^{QD}pT270 DNA from DNA tightropes.

Protein–QD complexes were excited at 488 nm by a solid-state laser (Sapphire DPSS). The QD signal was split into two channels by a dichroic mirror (T605LPXR, Chroma), and the red signals passed through an optical filter (ET655/40 nm, Chroma) before being detected by an EMCCD camera (iXon DU897, Andor Technology). All videos were taken using an inverted microscope (Nikon Ti-E) with a 100× objective (APO TIRF, Nikon) at an exposure time of 50 ms/frame.

Prism-type total internal reflection fluorescence microscopy (TIRFM) imaging

PEG/biotin-PEG passivated quartz slides were used to construct home-built flow cells, as described previously (74). To avoid nonspecific binding of proteins and DNA inside the imaging chamber, we conducted PEGylation of the cover slide twice (75) and incubated the chamber with 1× Blocking Reagent (Sigma, 11096176001) and 5% Tween-20 (Sigma, P7949) for 10 min (76). The slides were functionalized by incubating the imaging chamber with 0.1 mg/ml streptavidin. Cy5- and biotin-labeled duplexed telomeric DNA containing six TTAGGG repeats (69 bp) was then attached to the slide surface through streptavidin–biotin interactions. After incubation of proteins with surface anchored telomeric Cy5-DNA, 5 nM telomeric Cy3-DNA or control DNA without biotin (59 bp) was mixed with the indicated amount of proteins and injected into the imaging chamber with additional 10-min incubation. The samples were imaged using a prism-type

TIRF microscope. Cy3 and Cy5 excitations were achieved using 532 nm and 640 nm lasers, respectively. The emission from fluorophores was collected through a water immersion objective (60×, 1.2 NA), and the signal was split by a Dual-View optical splitter with a 645 nm dichroic mirror. The green and red signals then passed through optical filters (585/70 bandpass filter for Cy3, 655 long-pass filter for Cy5) before being detected by an EMCCD camera (Cascade 512B, Photometrics). Movies at 100 ms/frame were collected using the following excitation sequence: (1) brief excitation of the Cy5 fluorophore (~2 s) to locate DNA molecules; (2) excitation of the Cy3 fluorophore (~2 min) to monitor DNA molecules bridged by proteins; (3) brief excitation of the Cy5 fluorophore (~2 s) to reveal whether Cy5 was photobleached. All experiments were performed at room temperature in an imaging buffer containing 20 mM HEPES, pH 7.9, 100 mM NaCl, 0.3 mM $MgCl_2$, 1 mM EDTA, 0.5 mM DTT, and 2% glucose (w/v), with the addition of an oxygen scavenging system containing 100 U/ml glucose oxidase, 1000 U/ml catalase, and the triplet-state quenching reagent (2 mM Trolox) (77). Each data set containing more than 2000 traces was collected from at least three independent experiments. Reported values are the average of the independent repeats, and error bars report the SEM of the independent repeats.

Direct telomerase assay

Telomerase assays were conducted in the absence or presence of 500 nM POT1 and 500 nM His-SUMO-TPP1N (AA 89–334), as indicated in the figure legend, and 5 nM γ^{32}P ATP (PerkinElmer) end-labeled primer (5′TTAGGGTTAGCGTTAGGG3′) designed to position POT1 at the 10-nt primer 5′ end (71, 78). Telomerase reactions (20 μl) contained 1× Human Telomerase Buffer and cellular-relevant dNTP concentrations (5.2 μM dGTP, 24 μM dATP, 29 μM dCTP, and 37 μM dTTP) as described previously (79). The reactions were incubated at 37 °C for 1 h and then terminated with 2 μl of 0.5 mM EDTA and heat inactivated at 65 °C for 20 min. An equal volume of loading buffer (94% formamide, 0.1× TBE, 0.1% bromophenol blue, 0.1% xylene cyanol) was added to the reaction eluent from the G-25 spin column. The reactions were heat denatured for 10 min at 100 °C and loaded onto a 14% denaturing polyacrylamide gel (7 M urea, 1× TBE) and electrophoresed for 90 min at constant 38 W. Samples were imaged using a Typhoon Phosphorimager (GE Healthcare).

Dynabeads protein G pull-down assay

Dynabeads (Invitrogen, 10003D, 30 μl) were washed with 50 μl buffer (20 mM HEPES, pH 7.9, 100 mM NaCl, 0.3 mM $MgCl_2$, 1 mM EDTA, and 0.5 mM DTT) 3 times before use. Primary HA antibody (2.5 μg), TIN2L (2 μg), and TPP1N (His-SUMO-TPP1N or untagged TPP1N, 2 μg) were incubated with washed Dynabeads step by step. A magnetic stand was used to pull down the beads, and the beads were washed with 50 μl buffer twice between steps. Final elution of proteins from the beads was carried out in 1× NuPAGE LDS loading buffer (Life Technologies, NP0007) by heating up the samples to 80 °C for 10 min. All samples were run on an SDS-PAGE gel at 100 V for 50 min. The mass spectrometry analysis was performed on an Exploris 480 at the Molecular Education, Technology and Research Innovation Center (METRIC, North Carolina State University).

Statistical analysis

Data obtained from AFM, TIRFM imaging, and the DNA tightrope assay were from at least two to three independent experiments. The numbers reported are mean ± SEM, unless stated otherwise. The statistical significance level based on one-way ANOVA with Tukey's test for *post-hoc* analysis was set at $p < 0.05$ (SPSS version 27, IBM).

Data availability

All data are contained within the article and the supporting information.

Supporting information—This article contains supporting information.

Acknowledgments—We would like to thank the Xu groups at North Carolina State University, the Opresko group at the University of Pittsburgh, and the Smith group at New York University for technical support. This work was performed in part by the Molecular Education, Technology and Research Innovation Center (METRIC) at NC State University, which is supported by the State of North Carolina. Funding for open access charge: National Institutes of Health (R01GM123246).

Author contributions—P. L. O. and H. W. conceptualization; H. P., P. K., R. B., A. C. D., S. S., M. L., P. X., C. M., Q. T., P. H., C. Y., X. G.,W. L., and G. X. data curation; H. P., P. K., R. B., A. C. D., S. S., M. L., P. X., C. M., Q. T., P. H., D. B., and C. Y. formal analysis; K. W., R. R., and H. W. methodology; J. P., K. W., R. R., and H. W. project administration; G. X. resources; H. W. and P. L. O. supervision; H. P., P. L. O., and H. W. writing–original draft; K. W., R. R., P. L. O., and H. W. writing–review and editing.

Funding and additional information—This work was supported by the National Institutes of Health (R01GM107559 to H. W., R. R., R01GM123246 to H. W., R. R., and P. L. O, P30 ES025128 Pilot Project Grant to H. W. and P. K. through the Center for Human Health and the Environment at NCSU, R01CA207342 to P.L.O., and R01GM132263 to K.W.). The content is solely the responsibility of the authors and does not necessarily represent the official views of the National Institutes of Health.

Conflict of interest—The authors declare that they have no conflicts of interest with the contents of this article.

Abbreviations—The abbreviations used are: AFM, atomic force microscopy; alt-NHEJ, alternative nonhomologous end-joining; DDR, DNA damage response; EMSA, electrophoresis mobility shift assay; NHEJ, nonhomologous end-joining; QD, quantum dot; SEC, size-exclusion chromatography; TIRFM, total internal reflection fluorescence microscopy.

References

1. Palm, W., and de Lange, T. (2008) How shelterin protects mammalian telomeres. *Annu. Rev. Genet.* **42**, 301–334
2. Muraki, K., Nyhan, K., Han, L., and Murnane, J. P. (2012) Mechanisms of telomere loss and their consequences for chromosome instability. *Front. Oncol.* **2**, 135
3. de Lange, T. (2018) Shelterin-mediated telomere protection. *Annu. Rev. Genet.* **52**, 223–247
4. Wright, W. E., Tesmer, V. M., Huffman, K. E., Levene, S. D., and Shay, J. W. (1997) Normal human chromosomes have long G-rich telomeric overhangs at one end. *Genes Dev.* **11**, 2801–2809
5. Cech, T. R. (2004) Beginning to understand the end of the chromosome. *Cell* **116**, 273–279
6. Songyang, Z., and Liu, D. (2006) Inside the mammalian telomere interactome: Regulation and regulatory activities of telomeres. *Crit. Rev. Eukaryot. Gene Expr.* **16**, 103–118
7. Verdun, R. E., and Karlseder, J. (2007) Replication and protection of telomeres. *Nature* **447**, 924–931
8. Canudas, S., Houghtaling, B. R., Kim, J. Y., Dynek, J. N., Chang, W. G., and Smith, S. (2007) Protein requirements for sister telomere association in human cells. *EMBO J.* **26**, 4867–4878
9. Giraud-Panis, M. J., Pisano, S., Poulet, A., Le Du, M. H., and Gilson, E. (2010) Structural identity of telomeric complexes. *FEBS Lett.* **584**, 3785–3799
10. d'Adda di Fagagna, F., Reaper, P. M., Clay-Farrace, L., Fiegler, H., Carr, P., Von Zglinicki, T., Saretzki, G., Carter, N. P., and Jackson, S. P. (2003) A DNA damage checkpoint response in telomere-initiated senescence. *Nature* **426**, 194–198
11. Jaskelioff, M., Muller, F. L., Paik, J. H., Thomas, E., Jiang, S., Adams, A. C., Sahin, E., Kost-Alimova, M., Protopopov, A., Cadinanos, J., Horner, J. W., Maratos-Flier, E., and Depinho, R. A. (2011) Telomerase reactivation reverses tissue degeneration in aged telomerase-deficient mice. *Nature* **469**, 102–106
12. Broccoli, D., Chong, L., Oelmann, S., Fernald, A. A., Marziliano, N., van Steensel, B., Kipling, D., Le Beau, M. M., and de Lange, T. (1997) Comparison of the human and mouse genes encoding the telomeric protein, TRF1: Chromosomal localization, expression and conserved protein domains. *Hum. Mol. Genet.* **6**, 69–76
13. Broccoli, D., Smogorzewska, A., Chong, L., and de Lange, T. (1997) Human telomeres contain two distinct Myb-related proteins, TRF1 and TRF2. *Nat. Genet.* **17**, 231–235
14. Poulet, A., Pisano, S., Faivre-Moskalenko, C., Pei, B., Tauran, Y., Haftek-Terreau, Z., Brunet, F., Le Bihan, Y. V., Ledu, M. H., Montel, F., Hugo, N., Amiard, S., Argoul, F., Chaboud, A., Gilson, E., *et al.* (2012) The N-terminal domains of TRF1 and TRF2 regulate their ability to condense telomeric DNA. *Nucleic Acids Res.* **40**, 2566–2576
15. Griffith, J. D., Comeau, L., Rosenfield, S., Stansel, R. M., Bianchi, A., Moss, H., and de Lange, T. (1999) Mammalian telomeres end in a large duplex loop. *Cell* **97**, 503–514
16. Doksani, Y., Wu, J. Y., de Lange, T., and Zhuang, X. (2013) Super-resolution fluorescence imaging of telomeres reveals TRF2-dependent T-loop formation. *Cell* **155**, 345–356
17. Benarroch-Popivker, D., Pisano, S., Mendez-Bermudez, A., Lototska, L., Kaur, P., Bauwens, S., Djerbi, N., Latrick, C. M., Fraisier, V., Pei, B., Gay, A., Jaune, E., Foucher, K., Cherfils-Vicini, J., Aeby, E., *et al.* (2016) TRF2-Mediated control of telomere DNA topology as a mechanism for chromosome-end protection. *Mol. Cell* **61**, 274–286
18. Van Ly, D., Low, R. R. J., Frolich, S., Bartolec, T. K., Kafer, G. R., Pickett, H. A., Gaus, K., and Cesare, A. J. (2018) Telomere loop dynamics in chromosome end protection. *Mol. Cell* **71**, 510–525.e516
19. Sfeir, A., Kosiyatrakul, S. T., Hockemeyer, D., MacRae, S. L., Karlseder, J., Schildkraut, C. L., and de Lange, T. (2009) Mammalian telomeres resemble fragile sites and require TRF1 for efficient replication. *Cell* **138**, 90–103
20. Griffith, J., Bianchi, A., and de Lange, T. (1998) TRF1 promotes parallel pairing of telomeric tracts *in vitro*. *J. Mol. Biol.* **278**, 79–88
21. Lin, J., Countryman, P., Buncher, N., Kaur, P., E, L., Zhang, Y., Gibson, G., You, C., Watkins, S. C., Piehler, J., Opresko, P. L., Kad, N. M., and Wang, H. (2014) TRF1 and TRF2 use different mechanisms to find telomeric DNA but share a novel mechanism to search for protein partners at telomeres. *Nucleic Acids Res.* **42**, 2493–2504
22. Bianchi, A., Stansel, R. M., Fairall, L., Griffith, J. D., Rhodes, D., and de Lange, T. (1999) TRF1 binds a bipartite telomeric site with extreme spatial flexibility. *EMBO J.* **18**, 5735–5744
23. Kim, S. H., Kaminker, P., and Campisi, J. (1999) TIN2, a new regulator of telomere length in human cells. *Nat. Genet.* **23**, 405–412
24. Kim, S. H., Beausejour, C., Davalos, A. R., Kaminker, P., Heo, S. J., and Campisi, J. (2004) TIN2 mediates functions of TRF2 at human telomeres. *J. Biol. Chem.* **279**, 43799–43804
25. Houghtaling, B. R., Cuttonaro, L., Chang, W., and Smith, S. (2004) A dynamic molecular link between the telomere length regulator TRF1 and the chromosome end protector TRF2. *Curr. Biol.* **14**, 1621–1631
26. Kim, S. H., Davalos, A. R., Heo, S. J., Rodier, F., Zou, Y., Beausejour, C., Kaminker, P., Yannone, S. M., and Campisi, J. (2008) Telomere dysfunction and cell survival: Roles for distinct TIN2-containing complexes. *J. Cell Biol.* **181**, 447–460
27. O'Connor, M. S., Safari, A., Xin, H., Liu, D., and Songyang, Z. (2006) A critical role for TPP1 and TIN2 interaction in high-order telomeric complex assembly. *Proc. Natl. Acad. Sci. U. S. A.* **103**, 11874–11879
28. Ye, J. Z., Hockemeyer, D., Krutchinsky, A. N., Loayza, D., Hooper, S. M., Chait, B. T., and de Lange, T. (2004) POT1-interacting protein PIP1: A telomere length regulator that recruits POT1 to the TIN2/TRF1 complex. *Genes Dev.* **18**, 1649–1654
29. Hu, C., Rai, R., Huang, C., Broton, C., Long, J., Xu, Y., Xue, J., Lei, M., Chang, S., and Chen, Y. (2017) Structural and functional analyses of the mammalian TIN2-TPP1-TRF2 telomeric complex. *Cell Res.* **27**, 1485–1502
30. Chen, Y., Yang, Y., van Overbeek, M., Donigian, J. R., Baciu, P., de Lange, T., and Lei, M. (2008) A shared docking motif in TRF1 and TRF2 used for differential recruitment of telomeric proteins. *Science* **319**, 1092–1096
31. Kim, S. H., Han, S., You, Y. H., Chen, D. J., and Campisi, J. (2003) The human telomere-associated protein TIN2 stimulates interactions between telomeric DNA tracts *in vitro*. *EMBO Rep.* **4**, 685–691
32. Ye, J. Z., Donigian, J. R., van Overbeek, M., Loayza, D., Luo, Y., Krutchinsky, A. N., Chait, B. T., and de Lange, T. (2004) TIN2 binds TRF1 and TRF2 simultaneously and stabilizes the TRF2 complex on telomeres. *J. Biol. Chem.* **279**, 47264–47271
33. Takai, K. K., Kibe, T., Donigian, J. R., Frescas, D., and de Lange, T. (2011) Telomere protection by TPP1/POT1 requires tethering to TIN2. *Mol. Cell* **44**, 647–659
34. Frescas, D., and de Lange, T. (2014) Binding of TPP1 protein to TIN2 protein is required for POT1a,b protein-mediated telomere protection. *J. Biol. Chem.* **289**, 24180–24187
35. Pike, A. M., Strong, M. A., Ouyang, J. P. T., and Greider, C. W. (2019) TIN2 functions with TPP1/POT1 to stimulate telomerase processivity. *Mol. Cell. Biol.* **39**, e00593-18
36. Canudas, S., and Smith, S. (2009) Differential regulation of telomere and centromere cohesion by the Scc3 homologues SA1 and SA2, respectively, in human cells. *J. Cell Biol.* **187**, 165–173
37. Smith, S., Giriat, I., Schmitt, A., and de Lange, T. (1998) Tankyrase, a poly(ADP-ribose) polymerase at human telomeres. *Science* **282**, 1484–1487
38. Dynek, J. N., and Smith, S. (2004) Resolution of sister telomere association is required for progression through mitosis. *Science* **304**, 97–100
39. Kaminker, P. G., Kim, S. H., Desprez, P. Y., and Campisi, J. (2009) A novel form of the telomere-associated protein TIN2 localizes to the nuclear matrix. *Cell Cycle* **8**, 931–939
40. Smith, S. (2009) The long and short of it: A new isoform of TIN2 in the nuclear matrix. *Cell Cycle* **8**, 797–798
41. Chiang, Y. J., Kim, S. H., Tessarollo, L., Campisi, J., and Hodes, R. J. (2004) Telomere-associated protein TIN2 is essential for early embryonic development through a telomerase-independent pathway. *Mol. Cell. Biol.* **24**, 6631–6634
42. Savage, S. A., Giri, N., Baerlocher, G. M., Orr, N., Lansdorp, P. M., and Alter, B. P. (2008) TINF2, a component of the shelterin telomere protection complex, is mutated in dyskeratosis congenita. *Am. J. Hum. Genet.* **82**, 501–509
43. Walne, A. J., Vulliamy, T., Beswick, R., Kirwan, M., and Dokal, I. (2008) TINF2 mutations result in very short telomeres: Analysis of a large cohort

of patients with dyskeratosis congenita and related bone marrow failure syndromes. *Blood* **112**, 3594–3600
44. Takai, K. K., Hooper, S., Blackwood, S., Gandhi, R., and de Lange, T. (2010) *In vivo* stoichiometry of shelterin components. *J. Biol. Chem.* **285**, 1457–1467
45. Yang, Y., Wang, H., and Erie, D. A. (2003) Quantitative characterization of biomolecular assemblies and interactions using atomic force microscopy. *Methods* **29**, 175–187
46. Wang, H., Nora, G. J., Ghodke, H., and Opresko, P. L. (2011) Single molecule studies of physiologically relevant telomeric tails reveal POT1 mechanism for promoting G-quadruplex unfolding. *J. Biol. Chem.* **286**, 7479–7489
47. Kaur, P., Wu, D., Lin, J., Countryman, P., Bradford, K. C., Erie, D. A., Riehn, R., Opresko, P. L., and Wang, H. (2016) Enhanced electrostatic force microscopy reveals higher-order DNA looping mediated by the telomeric protein TRF2. *Sci. Rep.* **6**, 20513
48. Erie, D. A., and Weninger, K. R. (2014) Single molecule studies of DNA mismatch repair. *DNA Repair* **20**, 71–81
49. Lin, J., Countryman, P., Chen, H., Pan, H., Fan, Y., Jiang, Y., Kaur, P., Miao, W., Gurgel, G., You, C., Piehler, J., Kad, N. M., Riehn, R., Opresko, P. L., Smith, S., *et al.* (2016) Functional interplay between SA1 and TRF1 in telomeric DNA binding and DNA-DNA pairing. *Nucleic Acids Res.* **44**, 6363–6376
50. Countryman, P., Fan, Y., Gorthi, A., Pan, H., Strickland, J., Kaur, P., Wang, X., Lin, J., Lei, X., White, C., You, C., Wirth, N., Tessmer, I., Piehler, J., Riehn, R., *et al.* (2018) Cohesin SA2 is a sequence-independent DNA-binding protein that recognizes DNA replication and repair intermediates. *J. Biol. Chem.* **293**, 1054–1069
51. Pan, H., Jin, M., Ghadiyaram, A., Kaur, P., Miller, H. E., Ta, H. M., Liu, M., Fan, Y., Mahn, C., Gorthi, A., You, C., Piehler, J., Riehn, R., Bishop, A. J. R., Tao, Y. J., *et al.* (2020) Cohesin SA1 and SA2 are RNA binding proteins that localize to RNA containing regions on DNA. *Nucleic Acids Res.* **48**, 5639–5655
52. Wang, H., Yang, Y., and Erie, D. A. (2007) Characterization of protein-protein interactions using atomic force microscopy. In: Schuck, P., ed. *Protein Interactions Biophysical approaches for the Study of Complex Reversible Systems*, Springer Science+Business Media, LLC, Berlin, Germany: 39–78
53. Wang, H., DellaVecchia, M. J., Skorvaga, M., Croteau, D. L., Erie, D. A., and Van Houten, B. (2006) UvrB domain 4, an autoinhibitory gate for regulation of DNA binding and ATPase activity. *J. Biol. Chem.* **281**, 15227–15237
54. Chung, S. H., and Kennedy, R. A. (1991) Forward-backward non-linear filtering technique for extracting small biological signals from noise. *J. Neurosci. Methods* **40**, 71–86
55. Gauer, J. W., LeBlanc, S., Hao, P., Qiu, R., Case, B. C., Sakato, M., Hingorani, M. M., Erie, D. A., and Weninger, K. R. (2016) Single-molecule FRET to measure conformational dynamics of DNA mismatch repair proteins. *Methods Enzymol.* **581**, 285–315
56. Dunn, A. R., Kad, N. M., Nelson, S. R., Warshaw, D. M., and Wallace, S. S. (2011) Single Qdot-labeled glycosylase molecules use a wedge amino acid to probe for lesions while scanning along DNA. *Nucleic Acids Res.* **39**, 7487–7498
57. Hughes, C. D., Wang, H., Ghodke, H., Simons, M., Towheed, A., Peng, Y., Van Houten, B., and Kad, N. M. (2013) Real-time single-molecule imaging reveals a direct interaction between UvrC and UvrB on DNA tightropes. *Nucleic Acids Res.* **41**, 4901–4912
58. Kad, N. M., Wang, H., Kennedy, G. G., Warshaw, D. M., and Van Houten, B. (2010) Collaborative dynamic DNA scanning by nucleotide excision repair proteins investigated by single- molecule imaging of quantum-dot-labeled proteins. *Mol. Cell* **37**, 702–713
59. Pan, H., Bilinovich, S. M., Kaur, P., Riehn, R., Wang, H., and Williams, D. C., Jr. (2017) CpG and methylation-dependent DNA binding and dynamics of the methylcytosine binding domain 2 protein at the single-molecule level. *Nucleic Acids Res.* **45**, 9164–9177
60. Li, B., Qiao, R., Wang, Z., Zhou, W., Li, X., Xu, W., and Rao, Z. (2016) Crystal structure of a tankyrase 1-telomere repeat factor 1 complex. *Acta Crystallogr. F Struct. Biol. Commun.* **72**, 320–327
61. Ye, J. Z., and de Lange, T. (2004) TIN2 is a tankyrase 1 PARP modulator in the TRF1 telomere length control complex. *Nat. Genet.* **36**, 618–623
62. Erdel, F., Kratz, K., Willcox, S., Griffith, J. D., Greene, E. C., and de Lange, T. (2017) Telomere recognition and assembly mechanism of mammalian shelterin. *Cell Rep.* **18**, 41–53
63. Bandaria, J. N., Qin, P., Berk, V., Chu, S., and Yildiz, A. (2016) Shelterin protects chromosome ends by compacting telomeric chromatin. *Cell* **164**, 735–746
64. Timashev, L. A., Babcock, H., Zhuang, X., and de Lange, T. (2017) The DDR at telomeres lacking intact shelterin does not require substantial chromatin decompaction. *Genes Dev.* **31**, 578–589
65. Vancevska, A., Douglass, K. M., Pfeiffer, V., Manley, S., and Lingner, J. (2017) The telomeric DNA damage response occurs in the absence of chromatin decompaction. *Genes Dev.* **31**, 567–577
66. Bisht, K. K., Daniloski, Z., and Smith, S. (2013) SA1 binds directly to DNA through its unique AT-hook to promote sister chromatid cohesion at telomeres. *J. Cell Sci.* **126**, 3493–3503
67. Lim, C. J., Zaug, A. J., Kim, H. J., and Cech, T. R. (2017) Reconstitution of human shelterin complexes reveals unexpected stoichiometry and dual pathways to enhance telomerase processivity. *Nat. Commun.* **8**, 1075
68. Nelson, N. D., Dodson, L. M., Escudero, L., Sukumar, A. T., Williams, C. L., Mihalek, I., Baldan, A., Baird, D. M., and Bertuch, A. A. (2018) The C-terminal extension unique to the long isoform of the shelterin component TIN2 enhances its interaction with TRF2 in a phosphorylation- and dyskeratosis congenita cluster-dependent fashion. *Mol. Cell. Biol.* **38**, e00025-18
69. Opresko, P. L., von Kobbe, C., Laine, J. P., Harrigan, J., Hickson, I. D., and Bohr, V. A. (2002) Telomere-binding protein TRF2 binds to and stimulates the Werner and Bloom syndrome helicases. *J. Biol. Chem.* **277**, 41110–41119
70. Sowd, G., Wang, H., Pretto, D., Chazin, W. J., and Opresko, P. L. (2009) Replication protein A stimulates the Werner syndrome protein branch migration activity. *J. Biol. Chem.* **284**, 34682–34691
71. Wang, F., Podell, E. R., Zaug, A. J., Yang, Y., Baciu, P., Cech, T. R., and Lei, M. (2007) The POT1-TPP1 telomere complex is a telomerase processivity factor. *Nature* **445**, 506–510
72. Kocak, H., Ballew, B. J., Bisht, K., Eggebeen, R., Hicks, B. D., Suman, S., O'Neil, A., Giri, N., NCI DCEG Cancer Genomics Research Laboratory, NCI DCEG Cancer Sequencing Working Group, Maillard, I., Alter, B. P., Keegan, C. E., Nandakumar, J., and Savage, S. A. (2014) Hoyeraal-Hreidarsson syndrome caused by a germline mutation in the TEL patch of the telomere protein TPP1. *Genes Dev.* **28**, 2090–2102
73. Hanish, J. P., Yanowitz, J. L., and de Lange, T. (1994) Stringent sequence requirements for the formation of human telomeres. *Proc. Natl. Acad. Sci. U. S. A.* **91**, 8861–8865
74. LeBlanc, S. J., Gauer, J. W., Hao, P., Case, B. C., Hingorani, M. M., Weninger, K. R., and Erie, D. A. (2018) Coordinated protein and DNA conformational changes govern mismatch repair initiation by MutS. *Nucleic Acids Res.* **46**, 10782–10795
75. Chandradoss, S. D., Haagsma, A. C., Lee, Y. K., Hwang, J. H., Nam, J. M., and Joo, C. (2014) Surface passivation for single-molecule protein studies. *J. Vis. Exp.* **24**, 50549
76. Pan, H., Xia, Y., Qin, M., Cao, Y., and Wang, W. (2015) A simple procedure to improve the surface passivation for single molecule fluorescence studies. *Phys. Biol.* **12**, 045006
77. Roy, R., Hohng, S., and Ha, T. (2008) A practical guide to single-molecule FRET. *Nat. Methods* **5**, 507–516
78. Hwang, H., Buncher, N., Opresko, P. L., and Myong, S. (2012) POT1-TPP1 regulates telomeric overhang structural dynamics. *Structure* **20**, 1872–1880
79. Sanford, S. L., Welfer, G. A., Freudenthal, B. D., and Opresko, P. L. (2020) Mechanisms of telomerase inhibition by oxidized and therapeutic dNTPs. *Nat. Commun.* **11**, 5288